



VYSOKÉ UČENÍ TECHNICKÉ V BRNĚ

BRNO UNIVERSITY OF TECHNOLOGY

FAKULTA STROJNÍHO INŽENÝRSTVÍ

FACULTY OF MECHANICAL ENGINEERING

ÚSTAV FYZIKÁLNÍHO INŽENÝRSTVÍ

INSTITUTE OF PHYSICAL ENGINEERING

**KVANTOVÝ POPIS SUPERZÁŘIVOSTI EMITORŮ
S PLAZMONICKY ZPROSTŘEDKOVANOU
INTERAKCÍ**

QUANTUM DESCRIPTION OF SUPERRADIANCE OF EMITTERS WITH PLASMON-MEDIATED INTERACTION

DIPLOMOVÁ PRÁCE

MASTER'S THESIS

AUTOR PRÁCE

AUTHOR

Bc. Gabriela Olivíková

VEDOUCÍ PRÁCE

SUPERVISOR

Mgr. Vlastimil Křápek, Ph.D.

BRNO 2017

Zadání diplomové práce

Ústav:	Ústav fyzikálního inženýrství
Studentka:	Bc. Gabriela Olivíková
Studijní program:	Aplikované vědy v inženýrství
Studijní obor:	Fyzikální inženýrství a nanotechnologie
Vedoucí práce:	Mgr. Vlastimil Křápek, Ph.D.
Akademický rok:	2016/17

Ředitel ústavu Vám v souladu se zákonem č.111/1998 o vysokých školách a se Studijním a zkušebním řádem VUT v Brně určuje následující téma diplomové práce:

Kvantový popis superzářivosti emitů s plazmonicky zprostředkovanou interakcí

Stručná charakteristika problematiky úkolu:

Pojem superzářivost (superradiance) slouží v kvantové optice k popisu jevu, kdy systém vzájemně interagujících světelných zářičů vyzařuje díky vzájemné koherenci silněji, než odpovídá součtu příspěvků jednotlivých nezávislých zářičů.

V práci bude studován systém, v němž na sebe jednotlivé zářiče působí nejen přímo, ale také zprostředkovaně interakcí s plazmonickou částicí (malého kovového objektu s rozměry v řádu nanometrů nebo mikrometrů, v němž lze vybudit lokalizované kolektivní excitace plazmatu volných elektronů nazývané lokalizované plazmonové polaritony), v jejíž blízkosti jsou umístěny. Tímto způsobem se vytváří koherentní superpozice fotonů emitovaných z jednotlivých emitů odpovídajících superradiantnímu stavu.

Úkolem práce je vytvořit teoretický model, který bude popisovat emisi světla skupiny emitů silně vázaných k plazmonické částici. Model bude brát v úvahu reálné faktory ovlivňující emisi - zářivé a nezářivé rekombinační procesy vybuzených emitů, možnou variabilitu jednotlivých emitů a jejich interakce s plazmonickou částicí a interakci systému s prostředím, která se projeví nekoherentním vývojem fáze (tzv. dephasing). Budou stanoveny parametry modelu relevantní pro vznik superradiantního stavu a stanoven rozsah hodnot, pro něž takový stav vzniká. Jako vhodný výchozí bod pro vývoj modelu se jeví Lindbladův formalismus popisu otevřených kvantových systémů.

Cíle diplomové práce:

Vytvořit model popisující emisi vzájemně neinteragujících emitorů vázaných k centrální plazmonické částici.

Určit parametry důležité pro vznik superradiantního stavu.

Seznam literatury:

Novotny L. and Hecht B., Principles of nano-optics. Cambridge University Press, 1 ed., 2006.

Dicke R. H., Coherence in spontaneous radiation processes, Phys. Rev. 93, 99, 1954.

Pearle P., Simple derivation of the Lindblad equation, Eur. J. Phys. 33, 805, 2012.

Esteban R., Aizpurua J., and Bryant G. W., Strong coupling of single emitters interacting with phononic infrared antennae, New J. Phys. 16, 013052, 2014.

Termín odevzdání diplomové práce je stanoven časovým plánem akademického roku 2016/17

V Brně, dne

L. S.

prof. RNDr. Tomáš Šikola, CSc.
ředitel ústavu

doc. Ing. Jaroslav Katolický, Ph.D.
děkan fakulty

ABSTRACT

Superradiance is an enhanced decay of an excited system of emitters resulting from their mutual coupling. This thesis is focused on superradiance of the emitters coupled via their interaction with a plasmonic nanoparticle. So-called plasmon-mediated superradiance results in even stronger enhancement of the decay rate as the nanoparticle serves as an additional decay channel. We have developed a quantum model of the system of emitters coupled to a plasmonic nanoparticle, which allows us to differentiate between a pure dephasing and decay processes. We show that the pure dephasing can destroy the cooperative effect leading to superradiance. Furthermore, we have studied how the direct mutual coupling between emitters affects time evolution of the system in dependence on its configuration, and we show conditions when a decay of the system is dramatically decreased by direct coupling.

KEYWORDS

Superradiance, pure dephasing, strong coupling, weak coupling, plasmonics

ABSTRAKT

Superzářivost je zesílení rychlosti spontánní emise, které má původ ve vzájemné vazbě mezi emitory. Tato práce se zabývá superradiancí skupiny emitoreů, které jsou vzájemně vázány skrz plazmonickou nanočástici. Plasmonem zprostředkovaná superzářivost se projevuje výraznějším zesílením rychlosti spontánní emise, jelikož plazmonická částice poskytuje další možnost pro vyzáření energie. V rámci práce jsme vytvořili kvantový model systému emitoreů vázaných k plazmonické částici, který nám umožňuje rozlišit mezi náhodným rozfázováním emitoreů a jejich rekombinací. Práce ukazuje, že náhodné rozfázování může porušit kooperativní chování emitoreů, které vede k superradianci. Dále je v práci popsán efekt přímé vzájemné vazby mezi emitory na časový vývoj systému v závislosti na jeho konfiguraci a jsou stanoveny podmínky, při kterých systém vyzáruje výrazně pomaleji právě z důvodu přímé vzájemné vazby.

KLÍČOVÁ SLOVA

Supezářivost, náhodné rozfázování, silná vazba, slabá vazba, plazmonika

OLIVÍKOVÁ, Gabriela *Quantum description of superradiance of emitters with plasmon-mediated interaction*: master's thesis. Brno: Brno University of Technology, Faculty of Mechanical Engineering, Institute of Physical Engineering, 2017. 53 p. Supervised by Mgr. Vlastimil Křápek, Ph.D.

DECLARATION

I declare that I have elaborated my master's thesis on the theme of "Quantum description of superradiance of emitters with plasmon-mediated interaction" independently, under the supervision of Mgr. Vlastimil Křápek, Ph.D.

All sources, references and literature used or excerpted during the elaboration of this work are properly cited and listed in the complete reference.

Brno

.....

(author's signature)

ACKNOWLEDGEMENT

I would like to thank my supervisor Dr. Vlastimil Křápek for his inspiring comments and for corrections of this thesis. I would like to express my gratitude to Dr. Rubén Esteban and Prof. Javier Aizpurua for introducing me to the topic of superradiance and for possibility to spent several great months in their research group in San Sebastián. I highly appreciate help of Prof. Tomáš Šikola and Prof. Jiří Spousta with correcting this thesis. I thank Tomáš Neuman for all discussions about superradiance and related topics (and baking).

My gratitude definitely belongs to my family and friends, especially to my partner Vojta Schánilec, who always provide me with unfailing support and continuous encouragement.

Part of the work was carried out with the support of CEITEC Nano Research Infrastructure (MEYS CR, 2016–2019). Financial support from the FEI, which is now part of Thermo Fisher Scientific is gratefully acknowledged.

Gabriela Olivíková

CONTENTS

1	Introduction	1
2	Plasmon-emitter hybrid systems	3
2.1	Emitter	3
2.2	Plasmon	4
2.3	Quantum description of plasmon-emitter hybrid systems	6
2.3.1	Weak coupling regime and Purcell enhancement	7
2.3.2	Strong coupling	9
2.4	Excitation by classical light	10
3	Superradiance	12
3.1	Superradiance in absence of plasmon	12
3.2	Plasmon-mediated superradiance	14
4	Theoretical model	15
5	Symmetric configuration: weak coupling	19
5.1	Effect of initial state	19
5.2	Effect of pure dephasing	25
6	Symmetric configuration: strong coupling	28
7	Asymmetry in plasmon-emitter coupling strength	33
7.1	System of two groups of identical emitters	33
7.2	System of non-identical emitters	36
8	Effect of mutual coupling between emitters	40
9	Conclusion	46
	Appendices	48
A	Analytical solution for strong coupling	49
B	System of equations for asymmetrical case of two groups of emitters	51
	Bibliography	53

1 INTRODUCTION

In this thesis, we study how the emission from multiple emitters is influenced by their interaction with localized surface plasmons (i.e. surface plasmons bound to metallic nanoparticles). Surface plasmons are collective oscillations of the conduction electrons in metals resulting in strong enhancement of the electromagnetic field. Furthermore, surface plasmons have the ability to squeeze light into the nanometre scale and to enhance absorption and scattering of light [1, 2].

Localized surface plasmons supported by metallic nanoparticles can also enhance the emission rate from a nearby emitter, such as a quantum dot or a dye molecule. For a weak interaction between the emitter and the plasmon (the so-called weak coupling regime) the emitter decays by exciting the plasmon, which then reradiates the energy to the far field [3]. This enhancement of spontaneous emission is called the Purcell enhancement [4]. On the other hand, if the interaction between the plasmon and the emitter is strong enough, the energy that the emitter gives to the plasmon can be transferred back to the emitter, and the system enters the strong coupling regime [5, 6]. Symptomatic for strong coupling is an oscillatory evolution of populations of the emitter and plasmon, known as the Rabi oscillations [7].

An ensemble of N mutually coupled emitters (not coupled to any plasmon) is known to experience the phenomenon of superradiance. This effect has its origin in the coupling between the emitters, which results in the formation of cooperative states. One of these states, the superradiant or Dicke state [8], decays with an emission rate (per emitter) up to N times larger than the spontaneous decay rate of an individual emitter, whereas the decay rate of the other states, subradiant states, is decreased.

The present theoretical work studies a setup that combine superradiance with enhanced spontaneous emission by coupling an ensemble of emitters with a plasmonic particle. A simple classical model [9, 10] of such a system predicts a formation of the superradiant state with an enhancement of the decay rate given by the Purcell factor multiplied by the number of emitters. This classical model, however, ignores the phenomenon of pure dephasing – incoherent loss of phase without the emission of photon – which becomes very important at room temperature. Therefore, we have developed a quantum model, which incorporates pure dephasing. Besides that, effects of asymmetry (different properties of individual emitters) and random distribution of emitters can be studied using this model as well.

In Chapter 2 we describe a plasmon-emitter hybrid system – we address the effect of plasmon-enhanced spontaneous emission in the weak coupling regime and behaviour of a plasmon-emitter system in the strong coupling regime. Further, in Chapter 3 we introduce superradiance and its quantum description. In Chapter 4

we present the full model used for the description of superradiant emission from many single emitters coupled to a number of plasmon modes.

Following the introductory part, in Chapters 5–7 we discuss our results. After discussing the behaviour of the system with a symmetric configuration of emitters in the weak coupling regime in Chapter 5, we explore the behaviour of the system in the strong coupling regime in Chapter 6. Finally, in Chapter 7 we investigate the effect of asymmetry in emitter coupling strength. To study effects of asymmetry, we use a simple model of two groups of emitters identical within each group but otherwise different, and a more complex model of non-identical emitters, where the coupling strength between plasmon and each emitter depends on position of the emitter. In the latter, the effect of direct mutual coupling between two emitters is also studied.

2 PLASMON-EMITTER HYBRID SYSTEMS

Interaction between a plasmon and an emitter plays a crucial role in the effect of plasmon-mediated superradiance. In this section, we first introduce both a plasmon and an emitter independently with focus on the quantum description of each system. Next, the interaction between a plasmon and an emitter will be explained, and a quantum model of a plasmon-emitter hybrid system will be presented. In the following we will show two distinct regimes of plasmon-emitter systems – weak and strong coupling. Finally, we show how the illumination of a plasmon and an emitter can be introduced to the quantum model.

2.1 Emitter

We consider the emitter to be a system well described by two energy levels. Typically, this is the case of a quantum dot or fluorescent molecule undergoing dipolar transition between the lowest unoccupied and the highest occupied molecule orbital. Such a two-level system is described by a dipole moment operator [11]

$$\hat{\boldsymbol{\mu}} = \boldsymbol{\mu}\hat{\sigma}_+ + \boldsymbol{\mu}^*\hat{\sigma}_-, \quad (2.1)$$

where $\boldsymbol{\mu}$ is the transition dipole moment, $\hat{\sigma}_+$ and $\hat{\sigma}_-$ are the raising and lowering Pauli spin operators, respectively.

Excited emitter decays spontaneously to the ground state and emits a photon. This process called spontaneous emission is a transition between combined states of emitter and photon in the free space affected by a perturbation. Therefore, the probability of spontaneous emission per unit time γ_s (spontaneous decay rate) can be determined using Fermi's golden rule. This approach leads to following formula for spontaneous decay rate [12]

$$\gamma_s = \frac{\omega_s^3 |\boldsymbol{\mu}|^2}{3\pi\epsilon_0\hbar c^3}, \quad (2.2)$$

where ω_s is the transition frequency, ϵ_0 is the vacuum permitivity and c is the speed of light. Note, that for emission into a dielectric medium this equation holds with c being speed of light inside the medium.

Furthermore, energy of the emitter is given by the Hamiltonian

$$\hat{H}_{\text{em}} = \frac{1}{2}\hbar\omega_s\hat{\sigma}_z \quad (2.3)$$

with the Pauli operator $\hat{\sigma}_z = 2\hat{\sigma}_+\hat{\sigma}_- - 1$.

To describe dynamics of the emitter we use the master equation [13]

$$\frac{d\langle\hat{O}\rangle}{dt} = -\frac{i}{\hbar}\langle[\hat{O},\hat{H}]\rangle + \text{Tr}\left(\hat{O}\sum_i\hat{\mathcal{L}}_i\right), \quad (2.4)$$

which describes time evolution of an observable represented by the operator \hat{O} in open quantum system. In general, the losses to the environment are introduced by Lindblad operators $\hat{\mathcal{L}}_i$. Specifically, for emitter evolution, we use operator $\hat{\mathcal{L}}_s$ to incorporate spontaneous emission

$$\hat{\mathcal{L}}_s = -\frac{\gamma_s}{2}(\hat{\sigma}_+\hat{\sigma}_-\hat{\rho} + \hat{\rho}\hat{\sigma}_+\hat{\sigma}_- - 2\hat{\sigma}_-\hat{\rho}\hat{\sigma}_+), \quad (2.5)$$

where $\hat{\rho}$ is the density matrix.

Furthermore, the phase of the emitter interacting with an environment can relax with a rate γ_d , while the population of the emitter is sustained. This process is called pure dephasing and can be modelled by Lindblad operator $\hat{\mathcal{L}}_d$

$$\hat{\mathcal{L}}_d = -\gamma_d(\hat{\sigma}_+\hat{\sigma}_-\hat{\rho} + \hat{\rho}\hat{\sigma}_+\hat{\sigma}_- - 2\hat{\sigma}_+\hat{\sigma}_-\hat{\rho}\hat{\sigma}_+). \quad (2.6)$$

Typically, we study dynamics of the system by observing average population of the emitter expressed by the operator $\langle\hat{\sigma}_+\hat{\sigma}_-\rangle$.

2.2 Plasmon

Plasmon is a quantum of collective oscillation of conduction electrons in metals. Depending on the type of electron charge density contributing to oscillations we can distinguish two types of plasmons – volume and surface. Volume plasmons cannot be excited by light, therefore they are not of interest for study of light interactions with plasmon-emitters hybrid systems. On the contrary, surface charge density oscillations at metal-dielectric interface naturally couple to electromagnetic field and form surface plasmon polaritons (SPPs) [12].

Modes of electromagnetic (EM) field of SPPs are bound to metal-dielectric interface. In case of infinite interface SPPs are propagating modes with continuous dispersion relation. These modes can be excited by light if frequency and wave vector of the light match with SPP (otherwise energy or momentum conservation would be violated). This condition can be achieved using special techniques as Otto-Kretschmann configuration, scanning near-field optical microscopy (SNOM), or using grating. [2]

Metallic nanoparticles support special type of SPP, so called localized SPP (LSP), which can be excited by resonant light regardless the wave vector of incident

light. Beside that LSPs can radiate to far field, which results in typical feature of reflection (transmission) measurements of nanoparticles – a peak (dip) at resonant frequency of LSP. This fact can be explained as follows. LSP is a mode bound to a closed surface of a nanoparticle which thus acts as optical cavity, i.e., wave vector (and frequency) of LSP is limited to discrete values due to spatial restriction of EM mode of LSP. Also quantum mechanical description of LSP is equivalent to the treatment of optical cavity. Using a standard approach for quantization of EM field in cavity we can express electric field of LSP as [14]

$$\hat{\mathbf{E}}^s = \sqrt{\frac{\hbar\omega_0}{2\varepsilon_0 V_{\text{eff}}}} \left(\frac{\mathbf{E}^s(\mathbf{r})}{|\mathbf{E}_m^s|} \hat{a} + \frac{\mathbf{E}^{s*}(\mathbf{r})}{|\mathbf{E}_m^s|} \hat{a}^\dagger \right), \quad (2.7)$$

where ω_0 is the resonant frequency of LSP, $\mathbf{E}^s(\mathbf{r})$ is the scattered electric field at position \mathbf{r} and \mathbf{E}_m^s denotes the maximum value of the scattered field. Operators \hat{a} and \hat{a}^\dagger are the creation and the annihilation operators of cavity mode, respectively. Finally, V_{eff} is the effective volume of a plasmonic nanoparticle (equivalent of volume of optical cavity).

Let us consider total energy stored by the EM mode of LSP, which is in case of plasmonic structure equal to electric energy

$$W_E = \frac{1}{2} \int \Re \left\{ \frac{d[\omega\varepsilon(\mathbf{r},\omega)]}{d\omega} \right\} \Big|_{\omega=\omega_0} \hat{\mathbf{E}}^s \cdot \hat{\mathbf{E}}^s dV \quad (2.8)$$

$$= \frac{\hbar\omega_0}{4\varepsilon_0 V_{\text{eff}}} \int \Re \left\{ \frac{d[\omega\varepsilon(\mathbf{r},\omega)]}{d\omega} \right\} \Big|_{\omega=\omega_0} \left| \frac{\mathbf{E}^s(\mathbf{r})}{\mathbf{E}_m^s} \right|^2 (\hat{a}^\dagger \hat{a} + \hat{a} \hat{a}^\dagger) dV, \quad (2.9)$$

where ε denotes the dielectric function. As can be seen from Eq. (2.9), energy of LSP is expressed analogically to a harmonic oscillator with the Hamiltonian

$$\hat{H}_{\text{pl}} = \frac{\hbar\omega_0}{2} (\hat{a}^\dagger \hat{a} + \hat{a} \hat{a}^\dagger) = \hbar\omega_0 \left(\hat{a}^\dagger \hat{a} + \frac{1}{2} \right). \quad (2.10)$$

Energy stored in one plasmonic mode is indeed $\hbar\omega_0$, hence the effective volume of a nanoparticle can be determined by comparing Eqs. (2.9) and (2.10), which leads to

$$V_{\text{eff}} = \frac{\int \frac{1}{2} \Re \left\{ \frac{d[\omega\varepsilon(\mathbf{r},\omega)]}{d\omega} \right\} \Big|_{\omega=\omega_0} |\mathbf{E}^s(\mathbf{r})|^2 dV}{\varepsilon_0 |\mathbf{E}_m^s|^2}. \quad (2.11)$$

Important property of LSP is strong enhancement of the field in vicinity of the nanoparticle. In general, the local-field enhancement becomes stronger with sharper resonance, represented by the higher Q factor (quality factor). For the plasmonic nanoparticle with resonant frequency ω_0 , the Q factor can be determined from the dielectric function of the metal $\varepsilon(\omega) = \varepsilon'(\omega) + i\varepsilon''(\omega)$

$$Q = \frac{\omega_0 \left. \frac{d\varepsilon'(\omega)}{d\omega} \right|_{\omega=\omega_0}}{2\varepsilon''(\omega_0)}. \quad (2.12)$$

Generally, the Q factor is defined as a ratio between resonant frequency and bandwidth of resonance. Bandwidth of the resonance is directly related to finite lifetime ($1/\kappa$) of LSP. The decay rate of LSP is thus

$$\kappa = \frac{\omega_0}{Q}. \quad (2.13)$$

A standard way to include the LSP decay into master equation (2.4) is introducing a Lindblad term $\hat{\mathcal{L}}_p$

$$\hat{\mathcal{L}}_p = -\frac{\kappa}{2} (\hat{a}^\dagger \hat{a} \hat{\rho} + \hat{\rho} \hat{a}^\dagger \hat{a} - 2\hat{a} \hat{\rho} \hat{a}^\dagger). \quad (2.14)$$

As this thesis studies interaction of emitters with LSP, the term plasmon will be always used to refer to LSP in the following.

2.3 Quantum description of plasmon-emitter hybrid systems

In Sections 2.1 and 2.2 emitter and plasmon are described as independent systems. Interaction between these two elements can be easily understood as interaction of dipole moment with electric field – emitter is characterized by dipole moment operator $\hat{\boldsymbol{\mu}}$ and it is located in the near field of plasmon mode described by electric field operator $\hat{\mathbf{E}}^s$. Hamiltonian describing plasmon-emitter interaction is therefore

$$\hat{H}_{\text{pl-em}} = -\hat{\boldsymbol{\mu}} \cdot \hat{\mathbf{E}}^s \quad (2.15)$$

$$= -\sqrt{\frac{\hbar\omega_0}{2\varepsilon_0 V_{\text{eff}}}} \frac{1}{|\mathbf{E}_m^s|} (\boldsymbol{\mu} \hat{\sigma}_+ + \boldsymbol{\mu}^* \hat{\sigma}_-) \cdot (\mathbf{E}^s(\mathbf{r}) \hat{a} + \mathbf{E}^{s*}(\mathbf{r}) \hat{a}^\dagger). \quad (2.16)$$

In the interaction (or Heisenberg) picture, time dependence of the operators $\hat{\sigma}_+$ and \hat{a}^\dagger is $e^{i\omega t}$, the operators $\hat{\sigma}_-$ and \hat{a} have time dependence $e^{-i\omega t}$. The operators $\hat{\sigma}_+ \hat{a}^\dagger$ and $\hat{\sigma}_- \hat{a}$ therefore oscillate very fast in comparison with the terms $\hat{\sigma}_+ \hat{a}$ and $\hat{\sigma}_- \hat{a}^\dagger$. In a rotating wave approximation, the fast oscillating terms are neglected and the Hamiltonian has a simplified form

$$\hat{H}_{\text{pl-em}} = \hbar [g(\mathbf{r}) \hat{\sigma}_+ \hat{a} + g^*(\mathbf{r}) \hat{\sigma}_- \hat{a}^\dagger], \quad (2.17)$$

with $g(\mathbf{r})$ being

$$g(\mathbf{r}) = -\frac{\boldsymbol{\mu} \cdot \mathbf{E}^s(\mathbf{r})}{\hbar |\mathbf{E}_m^s|} \sqrt{\frac{\hbar\omega_0}{2\varepsilon_0 V_{\text{eff}}}}, \quad (2.18)$$

where $\mathbf{E}^s(\mathbf{r})$ is the scattered electric field of plasmonic nanoparticle at the position of the emitter. The spatial distribution of the emitter over the nanoparticle is thus introduced to the Hamiltonian by the parameter $g(\mathbf{r})$. However, for simplicity we will not consider a spatial dependence hereafter.

Plasmon-emitter system is then described by the so-called Jaynes-Cumming Hamiltonian [15, 16]

$$H = \hbar\omega_0 \left(\hat{a}^\dagger \hat{a} + \frac{1}{2} \right) + \frac{1}{2} \hbar\omega_s \hat{\sigma}_z + \hbar (g \hat{\sigma}_+ \hat{a} + g^* \hat{\sigma}_- \hat{a}^\dagger), \quad (2.19)$$

composed of the interaction Hamiltonian (2.17) and the terms describing plasmon [Eq. (2.10)] and emitter [Eq. (2.3)] separately. Dynamics of this system can be found using master equation (2.4) with the Lindblad terms describing a decay of the emitter [Eq. (2.5)] and plasmon [Eq. (2.14)], and pure dephasing of the emitter [Eq. (2.6)].

Furthermore, we assume that average populations of the ground state of both emitter and plasmon is always higher than average populations of the corresponding excited state, therefore

$$\langle \hat{\sigma}_z \rangle \approx -1, \quad \langle \hat{a}^\dagger \hat{a} \rangle - \langle \hat{a} \hat{a}^\dagger \rangle \approx -1. \quad (2.20)$$

This approximation, called weak illumination, leads to an effective reduction of the Hilbert space, so that the plasmon population $\langle \hat{a}^\dagger \hat{a} \rangle$, the emitter population $\langle \hat{\sigma}_+ \hat{\sigma}_- \rangle$ and coherences $\langle \hat{\sigma}_+ \hat{a} \rangle$, $\langle \hat{\sigma}_- \hat{a}^\dagger \rangle$ form a closed system of ordinary differential equations

$$\frac{d \langle \hat{a}^\dagger \hat{a} \rangle}{dt} = -\kappa \langle \hat{a}^\dagger \hat{a} \rangle + i (g \langle \hat{\sigma}_+ \hat{a} \rangle - g^* \langle \hat{\sigma}_- \hat{a}^\dagger \rangle), \quad (2.21)$$

$$\frac{d \langle \hat{\sigma}_+ \hat{a} \rangle}{dt} = - \left\{ \frac{\kappa + \gamma_s}{2} + \gamma_d - i(\omega_s - \omega_0) \right\} \langle \hat{\sigma}_+ \hat{a} \rangle - ig^* \langle \hat{\sigma}_+ \hat{\sigma}_- \rangle + ig^* \langle \hat{a}^\dagger \hat{a} \rangle, \quad (2.22)$$

$$\frac{d \langle \hat{\sigma}_- \hat{a}^\dagger \rangle}{dt} = - \left\{ \frac{\kappa + \gamma_s}{2} + \gamma_d + i(\omega_s - \omega_0) \right\} \langle \hat{\sigma}_- \hat{a}^\dagger \rangle + ig \langle \hat{\sigma}_+ \hat{\sigma}_- \rangle - ig \langle \hat{a}^\dagger \hat{a} \rangle, \quad (2.23)$$

$$\frac{d \langle \hat{\sigma}_+ \hat{\sigma}_- \rangle}{dt} = -i (g \langle \hat{\sigma}_+ \hat{a} \rangle - g^* \langle \hat{\sigma}_- \hat{a}^\dagger \rangle) - \gamma_s \langle \hat{\sigma}_+ \hat{\sigma}_- \rangle. \quad (2.24)$$

Time evolution of population of the emitter as given by this system of equations shows very different behaviour depending on the strength g characterizing the coupling between the plasmon and the emitter. Notably, one often differentiates between the weak and strong coupling regimes, which are described next. For plasmonic losses much larger than the spontaneous decay and the pure dephasing, the transition between both regimes occurs for $g \sim \kappa/4$.

2.3.1 Weak coupling regime and Purcell enhancement

When coupling between the plasmon and the emitter is weak compared to the plasmon decay, i.e., $g \lesssim \frac{\kappa}{4}$ (where $\kappa \gg \gamma_s, \gamma_d$), negligible energy is transferred from the

plasmon back to the emitter. The plasmon thus serves as additional decay channel and the emitter population continues to decay exponentially – as in the absence of plasmon – but with decay rate enhanced by the Purcell factor.

This effect can be more fundamentally explained by Fermi’s golden rule as follows. As was stated above, spontaneous emission is transition between combined states of emitter and photon. According to Fermi’s golden rule emission rate is proportional to the density of final states. Plasmon enhances density of electromagnetic states corresponding to final states of photon, and therefore spontaneous emission is enhanced. [12]

Let us now derive Purcell factor by solving Eqs. (2.21)–(2.24) in weak coupling limit. In the weak coupling regime, the plasmon reaches its equilibrium very fast compared to the time scale of the emitter decay, which allows us to assume, that at every instant the plasmon operators always correspond to a steady state, so that $d\langle\hat{\sigma}_+\hat{a}\rangle/dt = 0$, $d\langle\hat{\sigma}_-\hat{a}^\dagger\rangle/dt = 0$. This corresponds to the adiabatic approximation. Furthermore, in typical plasmonic systems in the weak coupling regime $\langle\hat{a}^\dagger\hat{a}\rangle \ll \langle\hat{\sigma}_+\hat{\sigma}_-\rangle$. Under this conditions Eqs. (2.21)–(2.24) are simplified to

$$\frac{d\langle\hat{\sigma}_+\hat{\sigma}_-\rangle}{dt} = - \left(\frac{2|g|^2 \left(\frac{\kappa + \gamma_s}{2} + \gamma_d \right)}{\left(\frac{\kappa + \gamma_s}{2} + \gamma_d \right)^2 + \Delta^2} + \gamma_s \right) \langle\hat{\sigma}_+\hat{\sigma}_-\rangle, \quad (2.25)$$

where $\Delta = \omega_s - \omega_0$ is the detuning between the plasmon and the emitter. The population of the emitter decays exponentially

$$\langle\hat{\sigma}_+\hat{\sigma}_-\rangle = e^{-\gamma t} \langle\hat{\sigma}_+\hat{\sigma}_-\rangle|_{t=0} \quad (2.26)$$

with the decay rate

$$\gamma = \frac{2|g|^2 \left(\frac{\kappa + \gamma_s}{2} + \gamma_d \right)}{\left(\frac{\kappa + \gamma_s}{2} + \gamma_d \right)^2 + \Delta^2} + \gamma_s. \quad (2.27)$$

Fig. 2.1 compares this analytical solution obtained within the adiabatic approximation to the numerical solution of Eqs. (2.21)–(2.24). We can observe that for the weak coupling regime the adiabatic approximation is valid and the analytical solution agrees well with the numerical simulation.

Using Eq. (2.27) we can directly define a generalized Purcell factor P_F^g corresponding to the increase of the decay rate with respect to the value γ_s of the spontaneous emission in vacuum [17]

$$P_F^g = \frac{\gamma}{\gamma_s} = \frac{2|g|^2 \left(\frac{\kappa + \gamma_s}{2} + \gamma_d \right)}{\gamma_s \left(\frac{\kappa + \gamma_s}{2} + \gamma_d \right)^2 + \Delta^2} + 1. \quad (2.28)$$

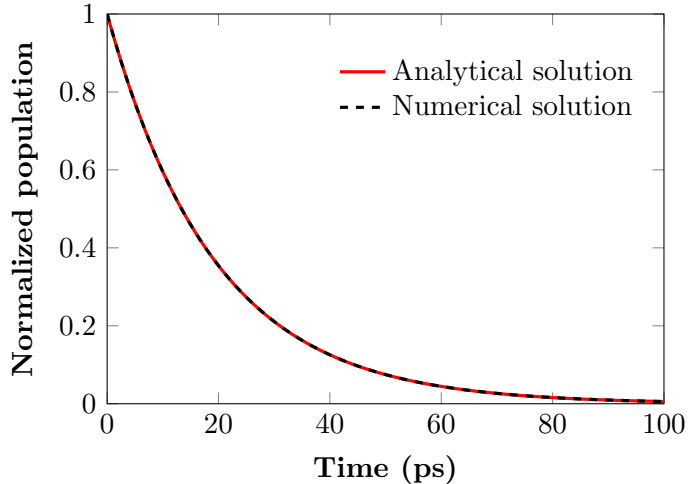


Fig. 2.1: Time evolution of the population of an emitter coupled to a plasmon mode in the weak coupling regime. The decay given by the generalized Purcell factor (red solid line) is compared with the numerical solution of Eqs. (2.21)–(2.24) (black dashed line). The parameters used for simulation are $\kappa = 3.14 \times 10^{14} \text{ s}^{-1}$, $\omega_0 = 3.14 \times 10^{15} \text{ s}^{-1}$, $\gamma_s = 1 \times 10^9 \text{ s}^{-1}$, $\gamma_d = 100\gamma_s$, $g = 0.2 \times 10^{13} \text{ s}^{-1} \approx 0.025\kappa/4$, $\Delta = 0 \text{ s}^{-1}$.

For $\kappa \gg \gamma_s$, $\kappa \gg \gamma_d$ and $\Delta = 0$, the Purcell factor simplifies to

$$P_F = \frac{4|g|^2}{\kappa\gamma_s} + 1. \quad (2.29)$$

Unless otherwise stated, when we give a value of the Purcell factor in the following we refer to the simplified Purcell factor.

This effect can be more fundamentally explained by Fermi's golden rule [12]. The spontaneous decay rate of the emitter is, according to Fermi's golden rule, proportional to the density of electromagnetic states, which is increased (compared to vacuum density of electromagnetic states) in vicinity of the plasmon.

2.3.2 Strong coupling

In the previous section, we found an exponential decay of an emitter coupled to a plasmon mode in the weak coupling regime. On the other hand, when the coupling strength $g \gtrsim \frac{\kappa}{4}, \frac{\gamma_s}{4}, \frac{\gamma_d}{4}$, we enter the strong coupling regime. In this case, the energy transferred from the emitter to the plasmon is only partly lost into environment but a substantial part is given back to the emitter, which results in a coherent exchange of energy between the plasmon and the emitter until dissipation occurs. This phenomenon is called Rabi oscillations.

Rabi oscillations can be observed in time evolution of the system given by Eqs. (2.21)–(2.24). Analytical solution for the case of no pure dephasing is provided in Appendix A. As the solution is rather complicated, we simplify it for the case when the decay rate of the emitter is negligible compared to the decay rate of the plasmon, $\gamma_s \ll \kappa$ and the emitter is in resonance with the plasmon ($\omega_0 = \omega_s$). Population of the emitter is then

$$\langle \hat{\sigma}_+ \hat{\sigma}_- \rangle = \frac{8|g|^2}{16|g|^2 - \kappa^2} \exp\left(-\frac{\kappa + \gamma_s}{2}t\right) \left[\cos\left(\sqrt{4|g|^2 - \frac{\kappa^2}{4}}t + \phi\right) + 1 \right], \quad (2.30)$$

where

$$\phi = \arctan \frac{\kappa \sqrt{16|g|^2 - \kappa^2}}{\kappa^2 - |8g|^2}. \quad (2.31)$$

Thus, the exponential decay of the emitter population with rate $(\kappa + \gamma_s)/2$ is modulated by oscillations of frequency $\sqrt{4|g|^2 - \kappa^2}/4$.

The analytical result is shown in Fig. 2.2 by the red line. Fig. 2.2 further shows the numerical solution of Eqs. (2.21)–(2.24) for different values of pure dephasing. We observe a perfect match of the analytical and numerical solution for zero dephasing ($\gamma_d = 0$). The black dotted and dash-dotted lines for $\gamma_d > 0$ show the effect of pure dephasing: increasing the pure dephasing decreases the amplitude and slightly increases the frequency of the oscillations.

2.4 Excitation by classical light

Typical way to excite a plasmon-emitter system in experiments is to illuminate the system by a plane wave. Interaction of the emitter with the plane wave can be describe as an interaction of its dipole moment with the electric field of the plane wave at the position of the emitter $\mathbf{E}^i(\mathbf{r})$, therefore the interaction Hamiltonian is

$$\hat{H}_{\text{cl-em}} = -(\boldsymbol{\mu} \hat{\sigma}_+ + \boldsymbol{\mu}^* \hat{\sigma}_-) \cdot \left(\frac{1}{2} \mathbf{E}^i(\mathbf{r}) e^{-i\omega t} + \frac{1}{2} \mathbf{E}^{i*}(\mathbf{r}) e^{i\omega t} \right) \quad (2.32)$$

As we are using the rotating wave approximation, the fast oscillating terms $\hat{\sigma}_+ e^{i\omega t}$ and $\hat{\sigma}_- e^{-i\omega t}$ can be neglected. Then the interaction Hamiltonian is

$$\hat{H}_{\text{cl-em}} = \hbar (\Omega e^{-i\omega t} \hat{\sigma}_+ + \Omega^* e^{i\omega t} \hat{\sigma}_-) \quad (2.33)$$

with Ω being

$$\Omega = -\frac{\boldsymbol{\mu} \cdot \mathbf{E}^i(\mathbf{r})}{2\hbar}. \quad (2.34)$$

The interaction Hamiltonian for a plasmon described by the bosonic operators can be written in analogy to Eq. (2.33)

$$\hat{H}_{\text{cl-pl}} = \hbar (f e^{-i\omega t} \hat{a}^\dagger + f^* e^{i\omega t} \hat{a}) \quad (2.35)$$

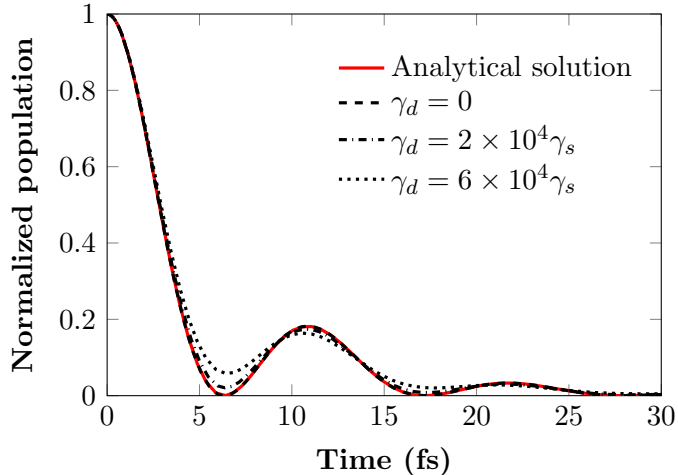


Fig. 2.2: Time evolution of the population of emitters coupled to a plasmon mode in the strong coupling regime. The analytical solution of Eqs. (2.21)–(2.24) for the case of no dephasing (red solid line) is compared with the numerical simulation for no dephasing (black dashed line), dephasing $\gamma_d = 2 \times 10^4 \gamma_s$ (black dotted line), and $\gamma_d = 6 \times 10^4 \gamma_s$ (black dash-dotted line). The parameters used for simulation are $\kappa = 3.14 \times 10^{14} \text{ s}^{-1}$, $\omega_0 = 3.14 \times 10^{15} \text{ s}^{-1}$, $\gamma_s = 1 \times 10^9 \text{ s}^{-1}$, $g = 0.3 \times 10^{15} \text{ s}^{-1}$, $\Delta = 0 \text{ s}^{-1}$.

The coupling constant f can be determined by comparing the scattered electric field of nanoparticle at the position \mathbf{r}_m of maximum amplitude (i. e. $\mathbf{E}^s(\mathbf{r}_m) = \mathbf{E}_m^s$)

$$\mathbf{E}^s(\mathbf{r}_m) = \frac{\mathbf{E}_m^s}{2} e^{-i\omega t} + \frac{\mathbf{E}_m^{s*}}{2} e^{i\omega t} \quad (2.36)$$

with the expectation value of the electric field operator $\langle \mathbf{E}^s(\mathbf{r}_m) \rangle$, Eq. (2.7), at the same position. For such a comparison, we determine value of the operator \hat{a} by applying the master equation (2.4) with the Hamiltonian (2.10) extended by the interaction term (2.35). Dissipative part of the master equation is formed by the Lindblad term (2.14). Equation for the annihilation operator \hat{a} is then

$$\frac{d\langle \hat{a} \rangle}{dt} = -i\omega_0 \langle \hat{a} \rangle - if e^{-i\omega t} - \frac{\kappa}{2} \langle \hat{a} \rangle, \quad (2.37)$$

which has a solution

$$\hat{a} = \frac{if}{i(\omega - \omega_0) - \kappa/2} e^{-i\omega t}. \quad (2.38)$$

The expectation value of the electric field operator $\langle \mathbf{E}^s(\mathbf{r}_m) \rangle$ for $\omega = \omega_0$ is then

$$\langle \mathbf{E}^s(\mathbf{r}_m) \rangle = -\sqrt{\frac{\hbar\omega_0}{2\varepsilon_0 V_{\text{eff}}}} \left(\frac{\mathbf{E}_m^s}{|\mathbf{E}_m^s|} \frac{2if}{\kappa} e^{-i\omega t} + \frac{\mathbf{E}_m^{s*}}{|\mathbf{E}_m^s|} \frac{2if^*}{\kappa} e^{i\omega t} \right). \quad (2.39)$$

By comparing Eqs. (2.36) and (2.39) we obtain the coupling constant f

$$f = i \frac{\kappa}{2} \sqrt{\frac{\varepsilon_0 V_{\text{eff}}}{2\hbar\omega_0}} |\mathbf{E}_m^s| \quad (2.40)$$

3 SUPERRADIANCE

Superradiance is an enhanced spontaneous emission, which results from a mutual interaction between emitters. The coupling between emitters gives rise to global states with decay rates different from those of the single emitters, and at least one of these states, so-called superradiant state, decays with a rate significantly enhanced with respect to the single emitter. [18]

Superradiance is typically observed in an ensemble of emitters confined in a volume with characteristic size much smaller than the radiation wavelength. In such case the emitters are coupled to each other directly, because they are all coupled to the common radiation field. Besides that, the coupling between emitters can be mediated by their interaction with another body, e.g., plasmonic nanoparticle. We show in the following that a classical model of such a system predicts even stronger superradiant effect in comparison to the system of directly coupled emitters.

3.1 Superradiance in absence of plasmon

To introduce the superradiant effect in absence of a plasmon, we will first describe a system of two emitters coupled to a common radiation field, which allows us to derive analytical solution for the system of emitters with identical spontaneous decay rate and pure dephasing located at arbitrary positions. Two coupled emitters in the absence of any plasmonic mode are described by the following Hamiltonian and Lindblad operators [19].

$$\hat{H} = \frac{1}{2}\hbar \sum_{i=1}^2 \omega_s^i \hat{\sigma}_z^i + \hbar \sum_{\substack{i,j=1 \\ i \neq j}}^2 \omega_c^{ij} \hat{\sigma}_+^i \hat{\sigma}_-^j, \quad (3.1)$$

$$\hat{\mathcal{L}}_s = -\frac{1}{2} \sum_{i=1}^2 \gamma_s^i (\hat{\sigma}_+^i \hat{\sigma}_-^i \hat{\rho} + \hat{\rho} \hat{\sigma}_+^i \hat{\sigma}_-^i - 2\hat{\sigma}_-^i \hat{\rho} \hat{\sigma}_+^i), \quad (3.2)$$

$$\hat{\mathcal{L}}_d = -\frac{1}{2} \sum_{i=1}^2 \gamma_d^i (\hat{\sigma}_+^i \hat{\sigma}_-^i \hat{\rho} + \hat{\rho} \hat{\sigma}_+^i \hat{\sigma}_-^i - 2\hat{\sigma}_+^i \hat{\sigma}_-^i \hat{\rho} \hat{\sigma}_+^i \hat{\sigma}_-^i), \quad (3.3)$$

$$\hat{\mathcal{L}}_c = -\frac{1}{2} \sum_{\substack{i,j=1 \\ i \neq j}}^2 \gamma_c^{ij} (\hat{\sigma}_+^i \hat{\sigma}_-^j \hat{\rho} + \hat{\rho} \hat{\sigma}_+^i \hat{\sigma}_-^j - 2\hat{\sigma}_-^j \hat{\rho} \hat{\sigma}_+^i), \quad (3.4)$$

where the first term in the Hamiltonian expresses the energy of the emitters, as in Eq. (2.3), and the Lindblad operators $\hat{\mathcal{L}}_s$ and $\hat{\mathcal{L}}_d$ describe the spontaneous decay and the pure dephasing of the single emitters, respectively, as in Eqs. (2.5) and (2.6). The coupling between the emitters is incorporated by the second term of the Hamiltonian with coupling constants ω_c^{ij} [20]

$$\omega_c^{ij} = \frac{3}{4} \sqrt{\gamma_s^i \gamma_s^j} \left\{ - [(\mathbf{e}_{\mu,i} \cdot \mathbf{e}_{\mu,j}) - (\mathbf{e}_{\mu,i} \cdot \mathbf{e}_r)(\mathbf{e}_{\mu,j} \cdot \mathbf{e}_r)] \frac{\cos \xi}{\xi} + [(\mathbf{e}_{\mu,i} \cdot \mathbf{e}_{\mu,j}) - 3(\mathbf{e}_{\mu,i} \cdot \mathbf{e}_r)(\mathbf{e}_{\mu,j} \cdot \mathbf{e}_r)] \times \left[\frac{\sin \xi}{\xi^2} - \frac{\cos \xi}{\xi^3} \right] \right\}, \quad (3.5)$$

and by the Lindblad operator $\hat{\mathcal{L}}_c$ with decay rates [20]

$$\gamma_c^{ij} = \frac{3}{4} \sqrt{\gamma_s^i \gamma_s^j} \left\{ [(\mathbf{e}_{\mu,i} \cdot \mathbf{e}_{\mu,j}) - (\mathbf{e}_{\mu,i} \cdot \mathbf{e}_r)(\mathbf{e}_{\mu,j} \cdot \mathbf{e}_r)] \frac{\sin \xi}{\xi} + [(\mathbf{e}_{\mu,i} \cdot \mathbf{e}_{\mu,j}) - 3(\mathbf{e}_{\mu,i} \cdot \mathbf{e}_r)(\mathbf{e}_{\mu,j} \cdot \mathbf{e}_r)] \times \left[\frac{\cos \xi}{\xi^2} - \frac{\sin \xi}{\xi^3} \right] \right\}, \quad (3.6)$$

where γ_s^i is the spontaneous decay rate of i -th emitter with the dipole moment $\boldsymbol{\mu}_i = \mu_i \mathbf{e}_{\mu,i}$. The parameter ξ is equal to $2\pi r_{ij}/\lambda_0$, where λ_0 is the resonant wavelength and r_{ij} is the distance between emitters. Finally, \mathbf{e}_r is the unit vector pointing from the i -th emitter to j -th emitter.

Utilizing the master equation (2.4), and the weak illumination approximation, Eq. (2.20), and assuming two identical emitters ($\gamma_s^1 = \gamma_s^2 = \gamma_s$, $\gamma_d^1 = \gamma_d^2 = \gamma_d$, $\gamma_c^{12} = \gamma_c^{21} = \gamma_c$, $\omega_s^1 = \omega_s^2$, $\omega_c^{12} = \omega_c^{21}$) excited in the same manner allows to consider $\langle \hat{\sigma}_+^1 \hat{\sigma}_-^1 \rangle = \langle \hat{\sigma}_+^2 \hat{\sigma}_-^2 \rangle$ and $\langle \hat{\sigma}_+^1 \hat{\sigma}_-^2 \rangle = \langle \hat{\sigma}_+^2 \hat{\sigma}_-^1 \rangle$, obtaining a simple system of equations for the emitter population

$$\frac{d \langle \hat{\sigma}_+^1 \hat{\sigma}_-^1 \rangle}{dt} = -\gamma_s \langle \hat{\sigma}_+^1 \hat{\sigma}_-^1 \rangle - \gamma_c \langle \hat{\sigma}_+^2 \hat{\sigma}_-^1 \rangle, \quad (3.7)$$

$$\frac{d \langle \hat{\sigma}_+^2 \hat{\sigma}_-^1 \rangle}{dt} = -\gamma_c \langle \hat{\sigma}_+^1 \hat{\sigma}_-^1 \rangle - (\gamma_s + 2\gamma_d) \langle \hat{\sigma}_+^2 \hat{\sigma}_-^1 \rangle. \quad (3.8)$$

Time evolution of the system is linear combination of two exponentials – one corresponds to a fast superradiant decay, and the other represents much slower subradiant decay. Decay rates given by eigenvalues of the system (3.7) and (3.8) are

$$\Gamma_{\text{sup}} = (\gamma_s + \gamma_d) + \sqrt{\gamma_d^2 + \gamma_c^2}, \quad (3.9)$$

$$\Gamma_{\text{sub}} = (\gamma_s + \gamma_d) - \sqrt{\gamma_d^2 + \gamma_c^2}. \quad (3.10)$$

This result shows that the decay rate of the emitter given by its spontaneous decay rate can be indeed either enhanced or decreased due to the coupling between emitters, resulting in a superradiant state with decay rate $\Gamma_{\text{sup}} > \gamma_s$ and a subradiant state with decay rate $\Gamma_{\text{sub}} < \gamma_s$.

The description of two coupled emitters can be easily extended to a system of N emitters. However, analytical solution can be provided only for the case of identical emitters aligned in same direction and located infinitesimally close to each other. Under these conditions $\gamma_c^{ij} = \gamma_s$ for all i, j , and population of each of the emitter is

determined by system of equations

$$\frac{d \langle \hat{\sigma}_+^i \hat{\sigma}_-^i \rangle}{dt} = -\gamma_s \langle \hat{\sigma}_+^i \hat{\sigma}_-^i \rangle - (N-1) \gamma_s \langle \hat{\sigma}_+^i \hat{\sigma}_-^j \rangle, \quad (3.11)$$

$$\frac{d \langle \hat{\sigma}_+^i \hat{\sigma}_-^j \rangle}{dt} = -\gamma_s \langle \hat{\sigma}_+^i \hat{\sigma}_-^i \rangle - [(N-1) \gamma_s + 2\gamma_d] \langle \hat{\sigma}_+^i \hat{\sigma}_-^j \rangle. \quad (3.12)$$

Additionally, for no dephasing the superradiant decay rate Γ_{sup} and subradiant decay rate Γ_{sub} have the value of

$$\Gamma_{\text{sup}} = N\gamma_s, \quad \Gamma_{\text{sub}} = 0. \quad (3.13)$$

This result is in agreement with the theory of superradiance introduced by Dicke [21].

3.2 Plasmon-mediated superradiance

Superradiance emerges also in case when all emitters are coupled to the same plasmonic nanoparticle. The plasmon-mediated coupling between the emitters is advantageous for two reasons. First, effective coupling of multiple emitters is possible as the coupling strength depends on plasmon-emitters distance. Providing equal distance between the plasmon and each of the emitters is easier than keeping equal distance between each pair of emitters. Second, if the coupling strength between the plasmon and the emitter corresponds to a weak coupling regime, superradiant effect is combined with Purcell enhancement, which results in a further enhancement of the decay rates. Classical model introduced by Pustovit and Shahbazyan [9] predicts superradiant decay rate

$$\Gamma_{\text{sup}} = N P_F^g \gamma_s, \quad (3.14)$$

where P_F^g is the generalized Purcell factor [see Eq. (2.28)]. Eq. (3.14) assumes an idealized direct coupling between emitters. Assuming that emitters couple only via the plasmon the resulting superradiance decay reads

$$\Gamma_{\text{sup}} = N (P_F^g - 1) \gamma_s + \gamma_s. \quad (3.15)$$

In the following, we develop a complex model describing a system of non-identical emitters. To study its properties we often utilize classical prediction (3.15).

4 THEORETICAL MODEL

In this thesis, we are interested in describing very general situations where an ensemble of emitters is coupled to a plasmon mode, possibly under a laser illumination and including the possibility of a strong pure dephasing. To study this situation, we first extend the simple models described in the previous section [Eqs. (2.5), (2.6), (2.14), (2.19) and (3.1)–(3.4)] to an arbitrary number of emitters M and plasmon modes N . Moreover, we incorporate the excitation of the system by a laser illumination, which leads to a more complex Hamiltonian

$$\begin{aligned} \hat{H} = & \hbar \sum_{k=1}^N \omega_0^k \left(\hat{a}^{k\dagger} \hat{a}^k + \frac{1}{2} \right) + \frac{\hbar}{2} \sum_{i=1}^M \omega_s^i \hat{\sigma}_z^i + \hbar \sum_{\substack{i,j=1 \\ i \neq j}}^M \omega_c^{ij} \hat{\sigma}_+^i \hat{\sigma}_-^j + \\ & + \hbar \sum_{k=1}^N \sum_{i=1}^M (g^{ik} \hat{\sigma}_+^i \hat{a}^k) + \hbar \sum_{k=1}^N (f^k e^{-i\omega t} \hat{a}^{k\dagger}) + \hbar \sum_{i=1}^M (\Omega^i e^{-i\omega t} \hat{\sigma}_+^i) + \text{h.c.} \end{aligned} \quad (4.1)$$

and Lindblad operators

$$\hat{\mathcal{L}}_p = -\frac{1}{2} \sum_{k=1}^N \kappa^k (\hat{a}^{k\dagger} \hat{a}^k \hat{\rho} + \hat{\rho} \hat{a}^{k\dagger} \hat{a}^k - 2\hat{a}^k \hat{\rho} \hat{a}^{k\dagger}), \quad (4.2)$$

$$\hat{\mathcal{L}}_s = -\frac{1}{2} \sum_{i=1}^M \gamma_s^i (\hat{\sigma}_+^i \hat{\sigma}_-^i \hat{\rho} + \hat{\rho} \hat{\sigma}_+^i \hat{\sigma}_-^i - 2\hat{\sigma}_-^i \hat{\rho} \hat{\sigma}_+^i), \quad (4.3)$$

$$\hat{\mathcal{L}}_c = -\frac{1}{2} \sum_{\substack{i,j=1 \\ i \neq j}}^M \gamma_c^{ij} (\hat{\sigma}_+^i \hat{\sigma}_-^j \hat{\rho} + \hat{\rho} \hat{\sigma}_+^i \hat{\sigma}_-^j - 2\hat{\sigma}_-^j \hat{\rho} \hat{\sigma}_+^i), \quad (4.4)$$

$$\hat{\mathcal{L}}_d = -\sum_{i=1}^M \gamma_d^i (\hat{\sigma}_+^i \hat{\sigma}_-^i \hat{\rho} + \hat{\rho} \hat{\sigma}_+^i \hat{\sigma}_-^i - 2\hat{\sigma}_+^i \hat{\rho} \hat{\sigma}_-^i). \quad (4.5)$$

The first term in the Hamiltonian and the Lindblad operator $\hat{\mathcal{L}}_p$ describe the energy and losses, respectively, of the plasmon modes with a frequency ω_0^k and a decay rate κ^k . The $\omega_s^i \hat{\sigma}_z^i$ terms in the Hamiltonian describe the transition energy of the two-level emitters, and $\hat{\mathcal{L}}_s$ the spontaneous decay of emitters with rates $\gamma^i = \gamma_s^i$. Furthermore, the $\omega_c^{ij} \hat{\sigma}_+^i \hat{\sigma}_-^j$ terms in the Hamiltonian for $i \neq j$ introduce the coupling between different emitters with a strength ω_c^{ij} . The $\hat{\mathcal{L}}_c^{ij}$ terms ($i \neq j$) introduce changes of the decay losses due to the emitter-emitter coupling via $\gamma^{ij} = \gamma_c^{ij}$ (see Section 3.1). Further, the Lindblad term $\hat{\mathcal{L}}_d$ describes pure dephasing of each emitter with rate γ_d^i . The last two terms in the Hamiltonian express the coupling of the system with photons described classically. These two terms introduce the excitation of the plasmon and emitters by the illumination with an efficiency given by the coupling strength f^k and Ω^i , respectively.

We consider the case of a weak illumination approximation $\hat{\sigma}_z \approx -1$ (see Section 2.3), giving the following finite system of equations for populations and coherences:

$$\begin{aligned} \frac{d\langle \hat{a}^{l\dagger} \hat{a}^m \rangle}{dt} = & \left[i(\omega_0^l - \omega_0^m) - \frac{\kappa^l + \kappa^m}{2} \right] \langle \hat{a}^{l\dagger} \hat{a}^m \rangle \\ & - i(f^m e^{-i\omega t} \langle \hat{a}^{l\dagger} \rangle - f^{l*} e^{i\omega t} \langle \hat{a}^m \rangle) \\ & + i \sum_{i=1}^M (g^{il} \langle \hat{\sigma}_+^i \hat{a}^m \rangle - g^{im*} \langle \hat{\sigma}_-^i \hat{a}^{l\dagger} \rangle), \end{aligned} \quad (4.6)$$

$$\frac{d\langle \hat{a}^l \rangle}{dt} = - \left(i\omega_0^l + \frac{\kappa^l}{2} \right) \langle \hat{a}^l \rangle - i f^l e^{-i\omega t} - i \sum_{i=1}^M g^{il*} \langle \hat{\sigma}_-^i \rangle, \quad (4.7)$$

$$\begin{aligned} \frac{d\langle \hat{\sigma}_+^m \hat{a}^l \rangle}{dt} = & - \left(i\omega_0^l + \frac{\kappa^l}{2} + \gamma_d^m \right) \langle \hat{\sigma}_+^m \hat{a}^l \rangle \\ & + \sum_{i=1}^M \left\{ \left(i\omega^{im} - \frac{\gamma^{im}}{2} \right) \langle \hat{\sigma}_+^i \hat{a}^l \rangle - i g^{il*} \langle \hat{\sigma}_+^m \hat{\sigma}_-^i \rangle \right\} \end{aligned} \quad (4.8)$$

$$\begin{aligned} & + i \sum_{k=1}^N g^{mk*} \langle \hat{a}^{k\dagger} \hat{a}^l \rangle - i (f^l e^{-i\omega t} \langle \hat{\sigma}_+^m \rangle - \Omega^{m*} e^{i\omega t} \langle \hat{a}^l \rangle), \\ \frac{d\langle \hat{\sigma}_+^m \hat{\sigma}_-^n \rangle}{dt} = & - \sum_{i=1}^M \left\{ \left(\frac{\gamma^{ni}}{2} + i\omega^{ni} \right) \langle \hat{\sigma}_+^m \hat{\sigma}_-^i \rangle + \left(\frac{\gamma^{im}}{2} - i\omega^{im} \right) \langle \hat{\sigma}_+^i \hat{\sigma}_-^n \rangle \right\} \\ & - (1 - \delta_{mn}) (\gamma_d^m + \gamma_d^n) \langle \hat{\sigma}_+^m \hat{\sigma}_-^n \rangle - i \sum_{k=1}^N (g^{nk} \langle \hat{\sigma}_+^m \hat{a}^k \rangle - g^{mk*} \langle \hat{\sigma}_-^n \hat{a}^{k\dagger} \rangle) \\ & - i (\Omega^n e^{-i\omega t} \langle \hat{\sigma}_+^m \rangle - \Omega^{m*} e^{i\omega t} \langle \hat{\sigma}_-^n \rangle), \end{aligned} \quad (4.9)$$

$$\frac{d\langle \hat{\sigma}_+^m \rangle}{dt} = i \sum_{k=1}^N g^{mk*} \langle \hat{a}^{k\dagger} \rangle - \sum_{i=1}^M \left(\frac{\gamma^{im}}{2} - i\omega^{im} \right) \langle \hat{\sigma}_+^i \rangle - \gamma_d^m \langle \hat{\sigma}_+^m \rangle - i\Omega^{m*} e^{i\omega t}. \quad (4.10)$$

In Chapters 5 and 6 we study symmetric configurations of the system – configurations where all parameters for all emitters are identical – and in Chapters 7 and 8, we study asymmetric configurations using two models. In the first model, we assume two different groups of emitters, where within each group all emitters are identical. Therefore, we distinguish operators and parameters related to these two groups of emitters by indices p and q . The number of emitters of each type is P and Q , respectively. This assumption leads to a system of 11 equations presented in Appendix B, which together with their complex conjugates describe an ensemble of arbitrary number of emitters [whereas the size of the system of Eqs. (4.6)–(4.10) grows as square of the number of particles, both plasmons and emitters, in the system]. The corresponding calculation code has been implemented and tested using

programme R [22], and it was used to obtain the results discussed in Chapters 5 and 6 and Section 7.1.

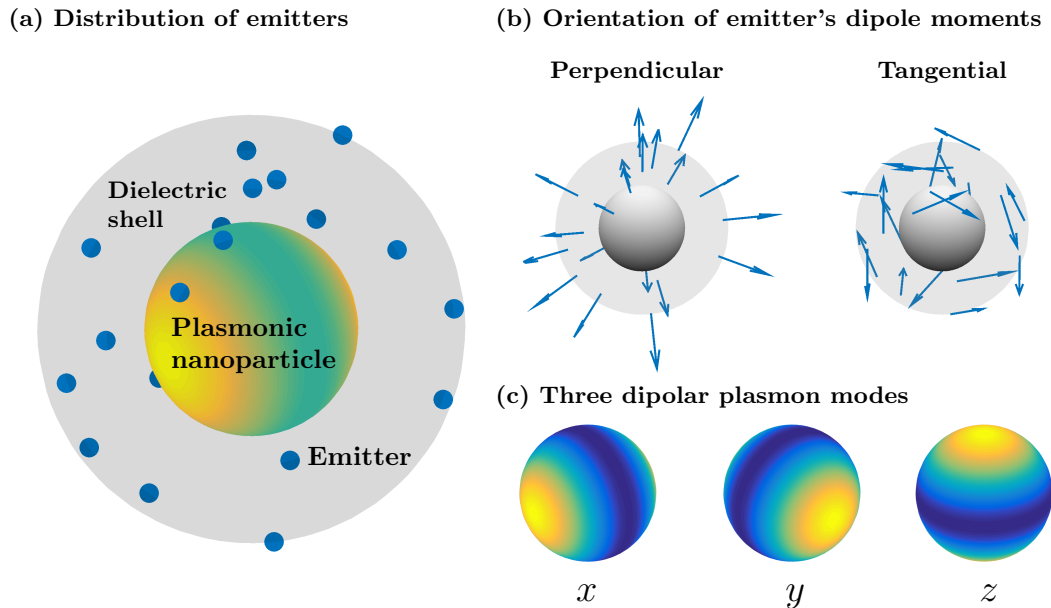


Fig. 4.1: (a) The system studied in Section 7.2 and Chapter 8 is composed of a plasmonic nanoparticle surrounded by a dielectric shell covered by an ensemble of randomly distributed emitters. (b) Emitters are characterized by dipole moments, whose orientation is considered to be either perpendicular or tangential with respect to the surface of the dielectric shell. (c) The nanoparticle is modelled as three dipolar modes – one in each of x , y and z directions.

The second model used to study asymmetric configurations utilizes directly Eqs. (4.6)–(4.10), whose numerical solution was retrieved with Matlab. As this model allows to describe emitters as non-identical, we can model more complex systems which require to consider the spatial distribution of the emitters. In this thesis, we study time evolution of the system composed of a spherical metal nanoparticle coupled to an ensemble of the emitters, which are separated from the nanoparticle by a dielectric shell with a relative permittivity ε_d , as it is shown in Fig. 4.1(a). For simplicity, we assume that the hybrid system is embedded in a dielectric medium with the same relative permittivity ε_d . Each emitter of the system is characterized by a dipole moment $\boldsymbol{\mu}$ and we study two kinds of system according to the orientation of emitters' dipole moments with respect to the surface of the dielectric shell – tangential and radial (perpendicular) – shown in Fig. 4.1(b).

We model the plasmonic nanoparticle as three dipolar modes with dipole moments $\mathbf{p}_x, \mathbf{p}_y, \mathbf{p}_z$ [see Fig. 4.1(c)] induced by incident electric field $\mathbf{E}^i = (E_x^i, E_y^i, E_z^i)$

as given by [23]

$$\mathbf{p}_\beta = \varepsilon_0 \alpha \mathbf{E}_\beta^i \mathbf{e}_\beta, \quad (4.11)$$

where \mathbf{e}_β is a unit vector in the direction $\beta = x, y, z$, ε_0 is vacuum permittivity and α is polarizability

$$\alpha = 3 \frac{\varepsilon_{NP}(\omega) - \varepsilon_d}{\varepsilon_{NP}(\omega) + 2\varepsilon_d} V \quad (4.12)$$

with $\varepsilon_{NP}(\omega)$ being dielectric function of the material of the nanoparticle at frequency of the incident light and V being volume of the nanoparticle. Note that a nanoparticle is at resonance if its polarizability is maximal, which requires

$$\Re\{\varepsilon_{NP}(\omega)\} + 2\varepsilon_d = 0. \quad (4.13)$$

To determine coupling strength $g^{i\beta}$ between i -th emitter and plasmon mode β , given by Eq. (2.18), we evaluate the electric field scattered by the plasmon mode at position of the emitter $\mathbf{r} = r\mathbf{e}_r$ with respect to the center of the nanoparticle using [23]

$$\mathbf{E}^s = \frac{1}{4\pi\varepsilon_0} \left\{ k^2 (\mathbf{e}_r \times \mathbf{p}_\beta) \times \mathbf{e}_r \frac{\exp(ikr)}{r} + [3\mathbf{e}_r (\mathbf{e}_r \cdot \mathbf{p}_\beta) - \mathbf{p}_\beta] \left(\frac{1}{r^3} - \frac{ik}{r^2} \right) \exp(ikr) \right\}, \quad (4.14)$$

where k is wave vector of scattered electromagnetic wave. Furthermore, we compute effective volume V_{eff} of the nanoparticle [Eq. (2.11)] using near field term of Eq. (4.14) (term proportional to $1/r^3$), we exclude far field terms as they diverge when r goes to infinity.

Coupling of the plasmon to the light f is dependent on parameters of the plasmonic resonance and intensity of the incident beam [see Eq. (2.40)], therefore in experiment we can achieve desired value of f by choosing suitable intensity of the incident light. Coupling strength between the emitter and the light Ω^i also depends on intensity of the incident light, and it can be determined using values of plasmon-light coupling f^β and plasmon-emitter coupling $g^{i\beta}$. From Eqs. (2.18), (2.34) and (2.40) we find

$$\Omega^i = -\frac{2i}{\kappa^\beta} \frac{\boldsymbol{\mu} \cdot \mathbf{E}^i}{\boldsymbol{\mu} \cdot \mathbf{E}^s} f^\beta g^{i\beta}. \quad (4.15)$$

Model of non-identical emitters is used in Section 7.2 to study effects of asymmetry in plasmon-emitter coupling strength and in Chapter 8 to study effect of direct coupling.

5 SYMMETRIC CONFIGURATION: WEAK COUPLING

We first study the emission from an ensemble of emitters coupled to a plasmon mode in a symmetric configuration, i.e., with all the emitters having identical properties including the coupling strength to the plasmonic particle g . Even though perfectly symmetric configurations cannot be achieved in realistic situations, they can provide important insights. Thus, we solve here the system of equations in Appendix B for the case in which all emitters are identical, including the same excitation, coupling with the plasmon g and the same pure dephasing γ_d and spontaneous decay rate $\gamma_s = 1 \times 10^9 \text{ s}^{-1}$. The emitters are coupled to the a plasmon mode with frequency $\omega_0 = 3.14 \times 10^{15} \text{ s}^{-1}$ (corresponding to wavelength $\lambda = 600 \text{ nm}$) and quality factor $Q = \omega_0/\kappa = 10$ [24]. We use coupling strength $g = 2.8 \times 10^{12} \text{ s}^{-1}$, which corresponds to a Purcell factor $P_F = 100$, as given by Eq. (2.29). These values are typical for plasmonic resonances [25] and correspond to the weak coupling regime for all the numbers of emitters N considered in this work. For simplicity, we assume that the emission energy of the emitters is equal to the energy of the plasmon resonance, i. e., the detuning equals to zero.

For simplicity we neglect the direct coupling between the emitters. We will include it into the model in Chapter 8.

5.1 Effect of initial state

The excitation of the system in experiment can be performed by different approaches. For example, it is possible to illuminate the particle with a short pulse of light of the adequate frequency to excite resonantly the plasmon. This approach can be naturally simulated by introducing a time dependent strength f of the coupling between the photon and the plasmon (see Section 2.4). Another possibility is to excite an emitter by high-frequency light into some higher excited state from which it rapidly decays into the lowest (metastable) excited state corresponding to the transition under study. This excitation can be simulated by setting the emitter's upper states populated without direct inclusion of the illumination.

The way of the excitation is expected to influence the dynamics of the studied system. In the following, we will demonstrate the effect of the excitation on the time evolution of the system for three different situations:

1. Plasmon in the ground state and emitters populated at $t = 0$, for no illumination ($f = 0$, $\Omega = 0$).

2. Plasmon populated and emitters in the ground state at $t = 0$, for no illumination ($f = 0$, $\Omega = 0$).
3. Plasmon and emitters initially in the ground state, illumination by a short pulse exciting the plasmonic mode ($\Omega = 0$, time dependent coupling strength $f(t)$ is modelled as a Gaussian function).

We always choose an initial state corresponding to a small enough population or a sufficiently weak laser illumination, so that the assumptions $\langle \hat{\sigma}_z \rangle \approx -1$ and $\langle \hat{a}^\dagger \hat{a} \rangle - \langle \hat{a} \hat{a}^\dagger \rangle \approx -1$, which were considered to obtain Eqs. (4.6)–(4.10), remain valid. In all cases we explore conditions where pure dephasing is negligible or appreciable, in order to explore to what extent this parameter – which does not have a simple classical equivalent – can affect the results.

First, we consider the case 1 with no illumination and initial population of the emitters (while the plasmon is in the ground state). Fig. 5.1(a) shows the time evolution of the population of the emitter with no pure dephasing as the total number of emitters in the system increases from 1 to 20. In the considered symmetrical configuration, all emitters will show identical behaviour. When a single emitter is coupled to the plasmon (blue line), it decays with spontaneous decay rate enhanced by the Purcell factor,¹ as expected (black dashed line corresponds to a simple exponential decay with rate $P_F^g \gamma_s$). However, as we increase the number of emitters, $N \geq 2$, we do not observe the expected superradiance, because initial state of populated emitters with coherences equal to zero does not correspond to pure superradiant state. In such case, we excite statistical mixture of one superradiant state with decay rate $N(P_F^g - 1)\gamma_s + \gamma_s$ and $N - 1$ subradiant states decaying with rate γ_s . Time evolution of normalized average population of single emitter is therefore

$$\langle \hat{\sigma}_+^m \hat{\sigma}_-^m \rangle = \frac{1}{N} \exp\{-[N(P_F^g - 1)\gamma_s + \gamma_s]t\} + \frac{N-1}{N} \exp(-\gamma_s t), \quad (5.1)$$

which is shown by black dash-dotted line in Fig. 5.1(a).

Next, we introduce a pure dephasing with a rate $\gamma_d = 10\gamma_s$. Fig. 5.1 (b) indicates that pure dephasing does not change the qualitative behaviour of the superradiant state, although it significantly increases the decay rate of the subradiant states. This increase of subradiant decay rate is more pronounced for a lower number of emitters. This can be intuitively explained in the following way. There is in total N distinct states of the system of the emitters, $(N - 1)$ being subradiant. The dephasing introduces transitions between these states with a rate γ_d , i.e., once per a time of $1/\gamma_d$ (on average) the system transforms into one of its N states, one of

¹Note that under the conditions studied in this section, the simplified [Eq. (2.29)] and generalized [Eq. (2.28)] Purcell factors are, in practice, identical. However, we refer to the generalized Purcell factor P_F^g if we take into account pure dephasing and to the simplified Purcell factor P_F if it refers to no pure dephasing.

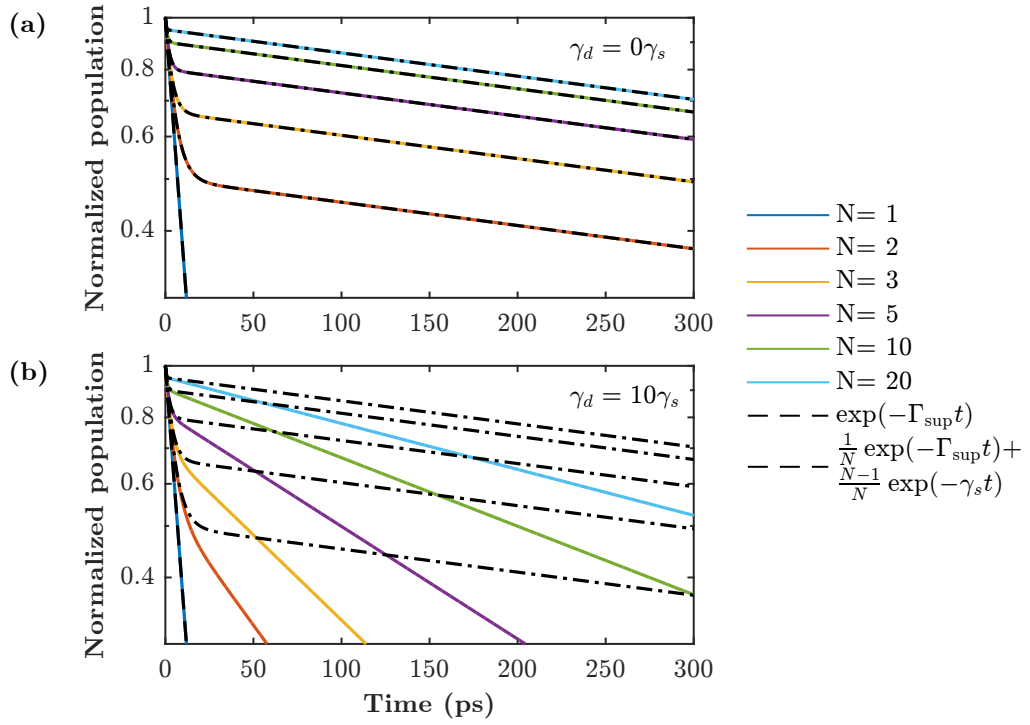


Fig. 5.1: Initial state – emitters populated: Time evolution of the normalized population of one emitter for different total number of emitters N between 1 and 20 for (a) no pure dephasing and (b) pure dephasing $\gamma_d = 10\gamma_s$. There is no illumination and initially the emitters are populated and the plasmon is in the ground state. The parameters used for simulation are $\gamma_s = 1 \times 10^9 \text{ s}^{-1}$, $\omega_0 = 3.14 \times 10^{15} \text{ s}^{-1}$, $\kappa = 3.14 \times 10^{14} \text{ s}^{-1}$, $\omega_s = \omega_0$, $P_F = 100$. The black dashed line indicates an exponential decay with rate $P_F^g \gamma_s$, corresponding to the single emitter coupled to the plasmon mode. The black dashed-dotted lines correspond to a statistical mixture of super- and subradiant states given by Eq. (5.1).

them superradiant. The probability that the final state will be superradiant is $1/N$, larger for smaller number of emitters.

Let us now consider the same system with initial conditions of the case 2 – the plasmon is initially populated while all emitters are in the ground state. Fig. 5.2(a) calculated for the case of no dephasing shows an exponential decay of the emitter population that becomes faster with increasing number of emitters. The results are in excellent agreement with the classical prediction (black dashed lines) showing that the emission is governed by superradiant collective states [9], as given by Eq. (3.15).

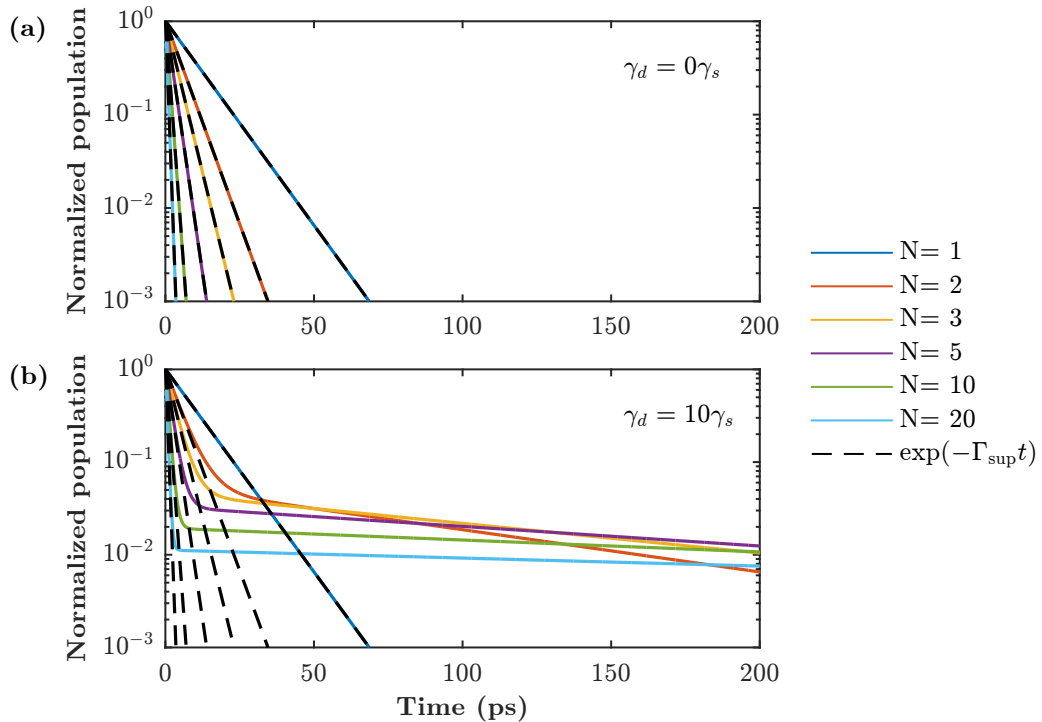


Fig. 5.2: Initial state – plasmon populated: Time evolution of the normalized population of one emitter for different total number of emitters N between 1 and 20 for (a) no pure dephasing and (b) pure dephasing $\gamma_d = 10\gamma_s$. There is no illumination and initially the emitters are in the ground state and the plasmon is populated. The parameters used for simulation are $\gamma_s = 1 \times 10^9 \text{ s}^{-1}$, $\omega_0 = 3.14 \times 10^{15} \text{ s}^{-1}$, $\kappa = 3.14 \times 10^{14} \text{ s}^{-1}$, $\omega_s = \omega_0$, $P_F = 100$. The black dashed line indicates an exponential decay with the rate given by the classical prediction, Eq. (3.15).

More intriguing behaviour appears when pure dephasing $\gamma_d = 10\gamma_s$ is introduced to the system [Fig. 5.2(b)]. Initially, only superradiant state is populated, and therefore the emitter decays as before – with decay rate proportional to $N(P_F^g - 1)\gamma_s + \gamma_s$. Due to pure dephasing, superradiant state decays into subradiant states, which gives rise to a statistical mixture of superradiant and subradiant states similar to Eq. (5.1),

but with different weights. In this case, the faster the superradiant state decays the lower is the population at which subradiant states start to dominate time evolution of the system. Moreover, as there are no cooperative states in case of single emitter, pure dephasing does not affect its decay as long as its influence on Purcell enhancement is negligible [see Eq. (2.28)]. Thus, after some time the population for a single emitter becomes smaller than for multiple emitters.

Finally, we study the effect of the number of emitters and pure dephasing on the system when initially all the emitters and the plasmon are in the ground state and the system is excited by laser illumination. All the other parameters are identical as those in Figs. 5.1 and 5.2. For this type of illumination, a coherent excitation pulse resonant with the plasmon excites the system. We are interested in the evolution of the population after the pulse has vanished. In our case, we simulate the laser pulse through the coupling f between photons and a plasmon (see Section 2.4), with the emitters being excited via their coupling with the plasmon. We ignore the direct excitation of the molecules ($\Omega = 0$), which is typically weaker. We model the pulse as a Gaussian function with standard deviation of 10 fs and intensity low enough to be in the weak illumination limit. The pulse reaches its maximum value at the time of 100 fs. Results are plotted in Fig. 5.3(a) for no pure dephasing and in Fig. 5.3(b) for pure dephasing $\gamma_d = 10\gamma_s$. For very short times we observe a very fast increase of the population that corresponds to the excitation of the emitter by the laser via the plasmon. When the plasmon is no longer excited, the emitter decays over the considerably larger time scale. Notably, the results are almost identical to those found for the case of initial population of plasmon in Fig. 5.2. In addition, we note, that the system evolves identically even for case when emitters are directly excited by light pulse ($\Omega \neq 0$) and the plasmon is not excited ($f = 0$).

Previous discussion of Figs. 5.1–5.3 implies that the simple classical prediction of superradiant decay rate [Eq. (3.15)] is valid regardless of the type of excitation. The reason why the excitation does not affect the decay rate of the superradiant state is that as far as we are interested in the time evolution after illumination the system of Eqs. (4.6)–(4.10) (see Chapter 4) describing dynamics of the studied system does not change. Thus, the decay of each mode of the system is unaffected by the illumination. However, the excitation can influence the initial condition, determining which modes have a stronger contribution to the time evolution, and thus to the emission of the system. We observe expected increment of decay rate with increasing number of emitters in time evolution of the system only if the initial state is satisfactorily described by a pure superradiant mode, which is the case when the system is excited via the plasmon or by the light illumination. The reason why illumination of either plasmon or emitters excites superradiant state is that light couples to superradiant state much more effectively than to subradiant states. On

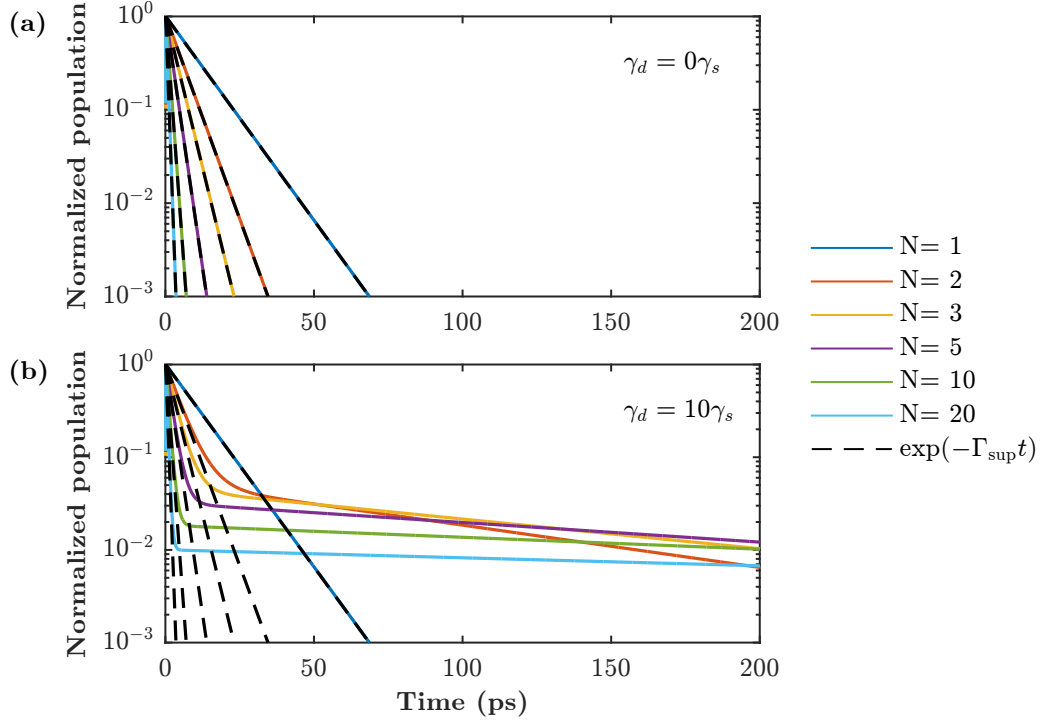


Fig. 5.3: Excitation of the plasmon by external illumination: Time evolution of the normalized population of one emitter for different total number of emitters N between 1 and 20 for (a) no pure dephasing and (b) pure dephasing $\gamma_d = 10\gamma_s$. Initially the emitters and the plasmon are in the ground state. Illumination of the system is provided by a Gaussian pulse with the standard deviation 10 fs and frequency resonant with the plasmon $\omega = 3.14 \times 10^{15} \text{ s}^{-1}$. The parameters used for simulation are $\gamma_s = 1 \times 10^9 \text{ s}^{-1}$, $\omega_0 = 3.14 \times 10^{15} \text{ s}^{-1}$, $\kappa = 3.14 \times 10^{14} \text{ s}^{-1}$, $\omega_s = \omega_0$, $P_F = 100$. The black dashed line indicates an exponential decay with the rate given by the classical prediction, Eq. (3.15).

the other hand, if all emitters are initially populated system is in the statistical mixture of all states and typical feature of superradiance – increase of the decay rate with increasing number of emitters – is not observed.

Furthermore, Figs. 5.1 and 5.2 show that due to pure dephasing any populated state decays into other states and populates them (such decay is additional to decay into environment). Therefore, the initial superradiant state becomes dephased after the time proportional to $1/(2N\gamma_d)$ and decay of the population becomes slower. In experiment, the description by the pure superradiant mode can still be relevant provided the decoherence applies only after the population of the emitter becomes undetectably small. On the other hand, for large pure dephasing, deviations from the simple description can become large, and the influence of the subradiant modes on the decay becomes apparent. The effect of stronger dephasing will be studied in more detail in the Section 5.2.

5.2 Effect of pure dephasing

Let us study in more detail the effect of pure dephasing on the system composed by 2 emitters and described by parameters stated at the beginning of Chapter 5. As time evolution of the system is given by linear combination of superradiant and subradiant states, we will discuss effect of pure dephasing on the system which is initially in one of these states. Superradiant initial state is modelled by initial condition when plasmon is in the ground state and populations and coherences of emitters are $\alpha/2$. Subradiant state is excited if populations of the emitters are $\alpha/2$, and their coherences are $-\alpha/2$. In both cases α is arbitrary real number much smaller than 1 [to fulfil conditions (2.20)].

First, we study the effect of weak dephasing (defined as $\gamma_d \leq P_F^g \gamma_s$, red and green lines in Fig. 5.4). Time evolution of the initially superradiant state is shown in Fig. 5.4(a), where we observe qualitatively same behaviour as in Figs. 5.2(b) and 5.3(b) – superradiant state characterized by the decay rate $N(P_F^g - 1)\gamma_s + \gamma_s$ decays due to pure dephasing into subradiant states, and therefore the decay of the emitter population becomes significantly slower. Moreover, Fig. 5.4(a) shows that contribution of subradiant states increases with increasing dephasing. At least half of the decay of the emitter population is yet dominated by the superradiant emission (notice the logarithmic scale) even for $\gamma_d = P_F \gamma_s = 100\gamma_s$.

Time evolution of the subradiant state of the system undergoing weak dephasing is shown in Fig. 5.4(b). This state starts to decay with rate γ_s , however, due to pure dephasing it populates also other states including superradiant state, and therefore decay of the emitter becomes faster. The resulting decay rate is identical with the

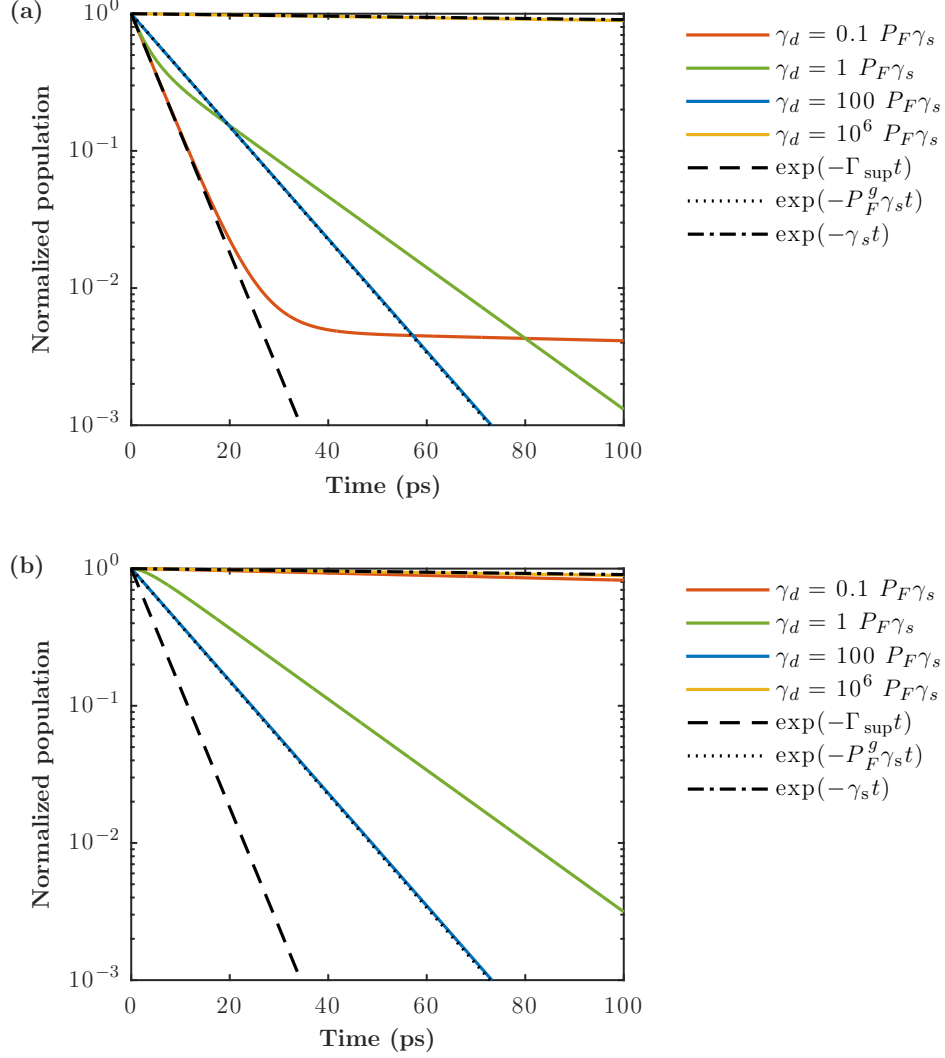


Fig. 5.4: Time evolution of the normalized population of one emitter in a system of $N = 2$ emitters for different values of pure dephasing. The system is initially in (a) a superradiant state or (b) a subradiant state. The parameters used for simulation are $\gamma_s = 1 \times 10^9 \text{ s}^{-1}$, $\omega_0 = 3.14 \times 10^{15} \text{ s}^{-1}$, $\kappa = 3.14 \times 10^{14} \text{ s}^{-1}$, $\omega_s = \omega_0$, and coupling strength $g = 2.8 \times 10^{12} \text{ s}^{-1}$ (corresponding to the Purcell factor $P_F = 100$ for low pure dephasing). The black dashed line shows an exponential decay with the rate equal to $N (P_F^g - 1) \gamma_s + \gamma_s$, the black dotted line indicates an exponential decay with rate $P_F^g \gamma_s$ and black dash-dotted line shows the exponential spontaneous decay rate γ_s .

corresponding one in time evolution of initially superradiant state [Fig. 5.4(a)].

Secondly, when pure dephasing is large, $\gamma_d \gg P_F \gamma_s$, system enters a regime, where the decay rate corresponds to $P_F^g \gamma_s$ (blue lines in Fig. 5.4). Thus, this situation is equivalent to having each emitter being coupled to the plasmon, but not to other emitters. As a result, time evolution of the system does not depend on the initial state, because both states correspond to same situation of a single emitter coupled to a plasmon mode. Note, that while for $\gamma_d = 10^4 \gamma_s = 100 P_F \gamma_s$ we obtain a decay $P_F^g \gamma_s$ (black dotted line), for $\gamma_d = 10^8 \gamma_s = 10^6 P_F \gamma_s$ (yellow line) the decay is γ_s (black dash-dotted line), because generalized Purcell factor is reduced to 1 when the pure dephasing is in the order of κ , as indicated by Eq. (2.28). This fact reflects that dephasing much larger than $P_F \gamma_s$ disables coupling between plasmon and emitter and emitter behaves independently on plasmon and other emitters.

To conclude, time evolution of the system of N emitters in the weak coupling regime is described by superposition of one superradiant state with decay rate $N(P_F^g - 1)\gamma_s + \gamma_s$ and $N - 1$ subradiant states with much slower decay rate. Pure dephasing and type of excitation determines the relative weights of superradiant state and subradiant states. Furthermore, depending on the type of excitation, system can be initially prepared either in a pure superradiant state or in a statistical mixture of super- and subradiant states. For both types of excitation pure dephasing acting on the system causes mixing of super- and subradiant states, which leads to change in the decay rate. The resulting decay rate depends on number of emitters and value of pure dephasing.

6 SYMMETRIC CONFIGURATION: STRONG COUPLING

This section is devoted to conditions for which the interaction strength is large enough to reach the strong coupling regime. We consider system in the symmetric configuration where all emitters behave identically, plasmon is initially populated and no illumination is considered. In the previous section, treating the weak coupling regime, the system often behaves as a single emitter with the spontaneous decay rate multiplied by the Purcell factor and the number of emitters. Such behaviour can be understood, if we consider a plasmon and an effective emitter (representing a system of N emitters) coupled with effective coupling strength

$$g^{\text{eff}} = \sqrt{N} |g|, \quad (6.1)$$

where g is coupling strength between the plasmon and one emitter. Using description of plasmon-emitter hybrid system presented in Section 2.3, we can expect that system of N emitters would enter strong coupling regime as the effective coupling overcomes the plasmonic losses, i.e., $g^{\text{eff}} > \kappa/4$.

In Fig. 6.1(a) we study the decay of the emitters for $N = 20$, for no dephasing and as a function of coupling strength g . We focus first on the behaviour of the emitter population after it reaches its maximum population, i.e., neglecting the initial phase in which the population of the emitters rises due to their excitation via the plasmon. For $g = 8.9 \times 10^{12} \text{ s}^{-1}$ ($g^{\text{eff}} = 0.13 \kappa$, blue line) and $g = 1.8 \times 10^{13} \text{ s}^{-1}$ ($g^{\text{eff}} = 0.25 \kappa$, red line), we observe an exponential decay typical for the weak coupling regime. However, if we further increase the coupling g , the system enters the strong coupling regime and Rabi oscillations can be observed in the decay of the emitter as shown by yellow ($g = 4.0 \times 10^{13} \text{ s}^{-1}$ corresponding to $g^{\text{eff}} = 0.53 \kappa$) and green ($g = 5.6 \times 10^{13} \text{ s}^{-1}$ corresponding to $g^{\text{eff}} = 0.80 \kappa$) lines.

As the effective coupling strength is given by $\sqrt{N} |g|$, we can expect that a similar effect can be achieved by increasing the number of emitters N . In Fig. 6.1(b) we plot the time evolution of the system for the same values of g^{eff} as in Fig. 6.1(a), but in this case the coupling g between the plasmon and the emitter is fixed to the value of $4 \times 10^{13} \text{ s}^{-1}$, while the number of emitters increases. Indeed, we can see that there is no apparent difference between these two situations, changing $|g|$ or N , as far as g^{eff} remains the same [compare lines of same colour in Fig. 6.1(a) and (b)].

We now briefly discuss the evolution of the emitter population in Fig. 6.1 during excitation (before it reaches the maximum). As we are considering no coupling of emitters to illuminating wave ($\Omega = 0$), the emitter is excited by the plasmon, and

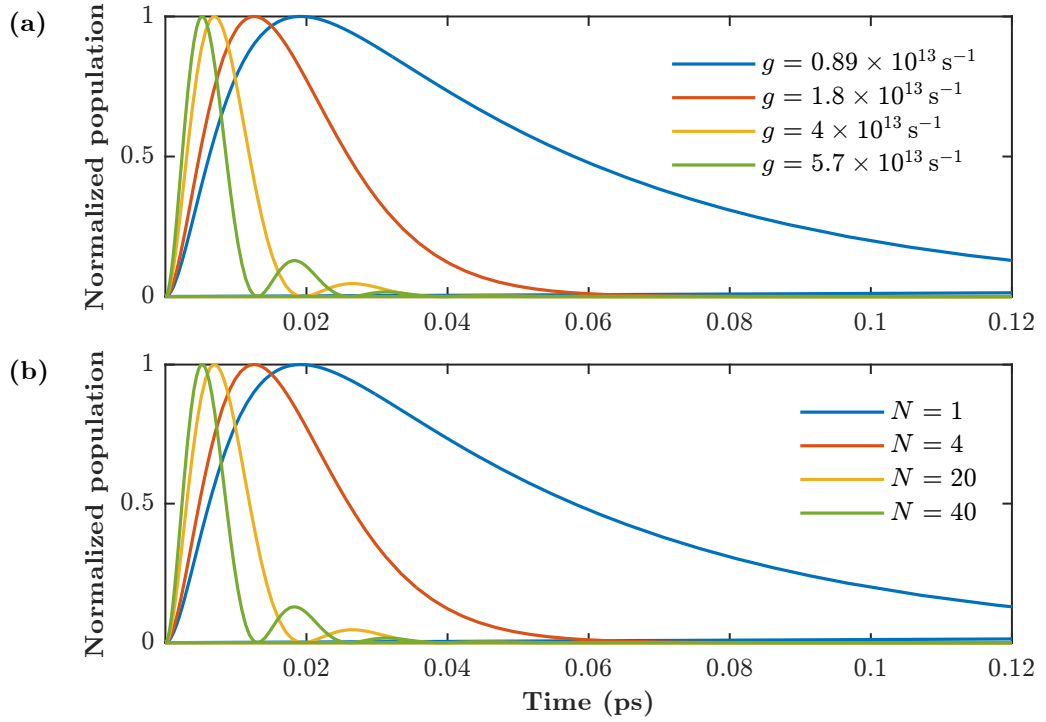


Fig. 6.1: Time evolution of the normalized emitter population for (a) 20 emitters and different values of the coupling strength g and for (b) $g = 4 \times 10^{13} \text{ s}^{-1}$ and a different number of emitters N . Each colour corresponds to same value of the effective coupling strength g_{eff} in both panels. The parameters used for the simulation are $\gamma_s = 1 \times 10^9 \text{ s}^{-1}$, $\gamma_d = 0 \text{ s}^{-1}$, $\omega_0 = 3.14 \times 10^{15} \text{ s}^{-1}$, $\kappa = 3.14 \times 10^{14} \text{ s}^{-1}$, $\omega_s = \omega_0$.

therefore, emitter population reaches maximum faster for stronger effective coupling between the plasmon and the emitter.

Next, we will consider the effect of pure dephasing on the population of the emitter when the system is in the strong coupling regime. Fig. 6.2 shows the decay of one of the $N = 20$ emitters, for different values of dephasing, and for the coupling strength $g = 2 \times 10^{14} \text{ s}^{-1}$ which corresponds the strong coupling regime ($g^{\text{eff}} = 2.85 \kappa$). For no dephasing (blue line) we observe clearly the Rabi oscillations – oscillations with the frequency of $\sqrt{4N|g|^2 - \kappa^2}/4$ – modified by the exponential decay (with the rate of $(\kappa + \gamma_s)/2$), which is in good agreement with the description of the strong coupling for a single emitter described in Section 2.3.2.

Pure dephasing affects time evolution of the emitter in two ways – it damps Rabi oscillations and changes the rate of exponential decay which modulates the oscillations. The latter is illustrated in Fig. 6.2, where the population of the emitter in case of no pure dephasing (blue line) decays much faster than in any case with non-zero pure dephasing. Thus, decay rate is decreased by introducing a weak pure dephasing. However, by further increasing the pure dephasing decay rate of the system is increased. This result is in agreement with the effects of pure dephasing found in the case of weak coupling – pure dephasing populates of subradiant states, which causes the sudden decrease of decay rate, and the subradiant states decays faster the larger is dephasing.

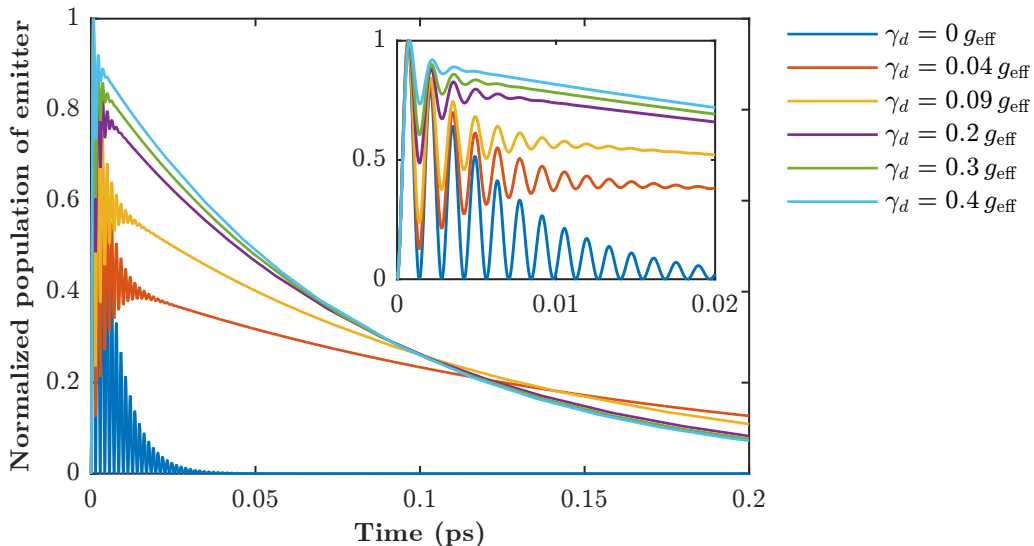


Fig. 6.2: Time evolution of the normalized emitter population for 20 emitters and different values of dephasing γ_d . The parameters used for the simulation are $\gamma_s = 1 \times 10^9 \text{ s}^{-1}$, $\omega_0 = 3.14 \times 10^{15} \text{ s}^{-1}$, $\kappa = 3.14 \times 10^{14} \text{ s}^{-1}$, $\omega_s = \omega_0$ and $g = 2 \times 10^{14} \text{ s}^{-1}$.

Fig. 6.2 further shows that with increasing dephasing Rabi oscillations become less pronounced and they diminish faster. To quantify the effect of damping we define visibility of the oscillations as

$$V = \frac{\max \langle \hat{\sigma}_+^p \hat{\sigma}_-^p \rangle - \min \langle \hat{\sigma}_+^p \hat{\sigma}_-^p \rangle}{\max \langle \hat{\sigma}_+^p \hat{\sigma}_-^p \rangle + \min \langle \hat{\sigma}_+^p \hat{\sigma}_-^p \rangle}. \quad (6.2)$$

In case of no dephasing the population of the emitter reaches zero at the minimum of the oscillations, implying perfect visibility $V = 1$. With increasing dephasing visibility decreases, as it is shown in Fig. 6.3(a) for different number of emitters in the system and (b) for different coupling strength g . Furthermore, visibility suddenly becomes zero as pure dephasing reaches values comparable with effective coupling strength. The fact that dependence of visibility of the oscillations on number of emitters and coupling strength is different even if the effective coupling strength is identical [same colour in Fig. 6.3(a) and (b)] implies that in case of pure dephasing systems with same effective coupling strengths but different number of emitters are no longer equivalent.

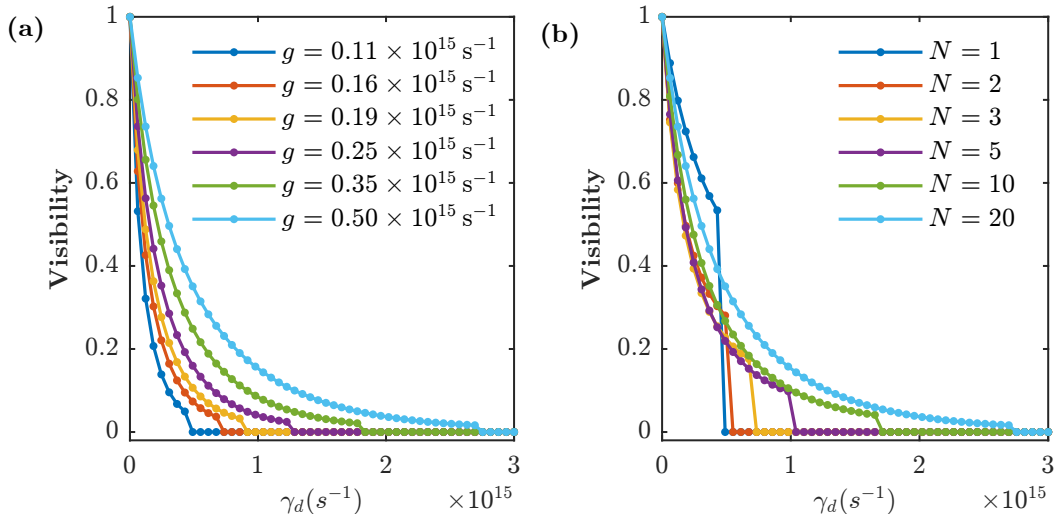


Fig. 6.3: Visibility of the Rabi oscillations as a function of pure dephasing γ_d for (a) $N = 20$ emitters and different coupling strength g and (b) for the coupling strength $g = 0.5 \times 10^{15} s^{-1}$ and different number of emitters N . Each colour corresponds to the same value of effective coupling in both graphs. The parameters used for the simulation are $\gamma_s = 1 \times 10^9 s^{-1}$, $\omega_0 = 3.14 \times 10^{15} s^{-1}$, $\kappa = 3.14 \times 10^{14} s^{-1}$, $\omega_s = \omega_0$.

To conclude, in the strong coupling regime a system of emitters with no pure dephasing behaves as an effective emitter coupled to a plasmon by the effective coupling strength proportional to the plasmon-emitter coupling strength and square root of number of emitters. Population of the emitter shows a typical feature of

strong coupling – Rabi oscillations. In addition, dephasing acts as a damping of Rabi oscillations. By analysis of the damping we found that systems with same effective coupling strength but different number of emitters are no longer equivalent if pure dephasing is present.

7 ASYMMETRY IN PLASMON-EMITTER COUPLING STRENGTH

In a realistic situation, when an ensemble of emitters is coupled to a plasmon mode supported by a metallic nanoparticle, an exact modelling of the system can be rather complicated, as it is not possible to perfectly control the position and orientation of the dipoles. Notably, the idealized symmetric configuration may not fully describe an experiment. In Section 7.1 we provide insights into the effects of asymmetry in the plasmon-emitter coupling strength using a model which assumes two different groups of emitters, where all emitters within each group are identical. Such a model does not increase too much the number of equations that describe the dynamics of the system, which allows better understanding of the results. However, such a model is still too simplified to describe experimental situations, and therefore we developed model where all emitters are considered to be non-identical. In Section 7.2 we utilize this model to study system of emitters randomly distributed over metal sphere covered by dielectric layer. We consider three plasmonic dipole modes of the sphere and coupling strength between each emitter and plasmon mode reflects the position and orientation of the emitter with respect to plasmon.

7.1 System of two groups of identical emitters

We study the effect of asymmetry in the coupling strength between the plasmon and the emitters in a system consisting of P emitters of type p and Q emitters of type q , where the total number of emitters $N = P+Q = 20$. The studied system is described by system of equations presented in Appendix B. To introduce the asymmetry in the coupling strength g , we first set a fixed value of g^q for the emitters of the type q . Then, we consider three different values of g^p given as multiples of g^q and the excitation of the system by a Gaussian pulse similar to the one used in Chapter 5 (with a standard deviation of 10 fs and its maximum value at 100 fs). We focus on the decay of the emitters of type p .

In Fig. 7.1 we show the case of no pure dephasing $\gamma_d = 0$. The different panels show results for different number P of emitters of type p . From top to bottom, we show results for P being (a) 25 %, (b) 50 %, (c) 75 % and (d) 100 % of the total number of emitters N . The last graph thus shows the symmetric situation where all emitters are of the same type p . The red line in all graphs shows the decay in the symmetric case $g^p = g^q$, while green and blue lines show the decay for asymmetric cases $g^p = 2g^q$ and $g^p = 3g^q$, respectively. We choose $g^q = 3 \times 10^{12} \text{ s}^{-1}$ (corresponding to $P_F = 115$) which corresponds to the weak coupling regime for

all values g^p and P . Indeed, in Fig. 7.1 we can observe that the decay remains exponential in all cases.

By looking at each single panel in Fig. 7.1, it is clear that with increasing g^p , the decay rate increases. On the other hand, comparing the different panels shows that, as the percentage of the emitters of type p in the system increases, the decay rate also increases (because of increased Purcell factor). Notice that the red line corresponds to $g^p = g^q$, so all emitters are in practice identical, and we need to compare the blue and green lines in the Fig. 7.1. In these two cases $g^p > g^q$, and thus increasing P corresponds to having a larger proportion of the emitters with larger coupling strength and faster emission.

As could be expected, by increasing the value of the coupling strength g of some of the emitters we obtain a faster decay. More quantitatively, from previous work [9] and the results in Chapter 5, we can expect the system to behave as a single emitter experiencing a superradiant decay with a rate

$$\Gamma_{\text{sup}}^{p,\text{eff}} = P (P_F^{g,p} - 1) \gamma_s^p + Q (P_F^{g,q} - 1) \gamma_s^q + \gamma_s^p, \quad (7.1)$$

where $P_F^{g,p}$ ($P_F^{g,q}$) is the generalized Purcell factor of a single emitter p (q) defined by Eq. (2.28). The corresponding effective Purcell factor is

$$P_F^{p,\text{eff}} = \frac{\Gamma_{\text{sup}}^{p,\text{eff}}}{\gamma_s^p}. \quad (7.2)$$

For no pure dephasing and $\gamma_s^p = \gamma_s^q$, Eq. (7.2) is equivalent to introducing an effective coupling strength $g^{\text{eff}} = \sqrt{P |g^p|^2 + Q |g^q|^2}$ consistently with Chapter 6. Notice, that we obtain the same effective Purcell factor for the two types of emitters. Following discussion in the Chapters 2 and 3, it is possible to interpret Eqs. (7.1) and (7.2) as reflecting the fact that the Purcell effect depends on the coupling strength between plasmon and emitters (as given by P_F^p and P_F^q) and that superradiance depends on the number of emitters involved (P and Q).

The black lines in Fig. 7.1 correspond to an exponential decay with decay rate $\Gamma_{\text{sup}}^{p,\text{eff}}$, given by Eq. (7.1), for $g^p = g^q$ (dashed line), $g^p = 1.5g^q$ (dotted line), $g^p = 2g^q$ (dash-dotted line). It is apparent that the numerical results are in very good agreement with Eq. (7.1), so that this simple description is valid for configuration with asymmetry in the coupling strength and no pure dephasing.

Next, we study the effect of a pure dephasing in the asymmetric system (composed of p -type and q -type emitters). In Fig. 7.2, we show the decay of the emitter's population with time as a function of asymmetry parameters g^p (decay rate of the p -type emitters) and P (number of the p -type emitters). The values of all other parameters are the same as in the previous case (related to Fig. 7.1). The value of the pure dephasing reads $\gamma_d^p = \gamma_d^q = 10\gamma_s$. We can see that the emitter is initially

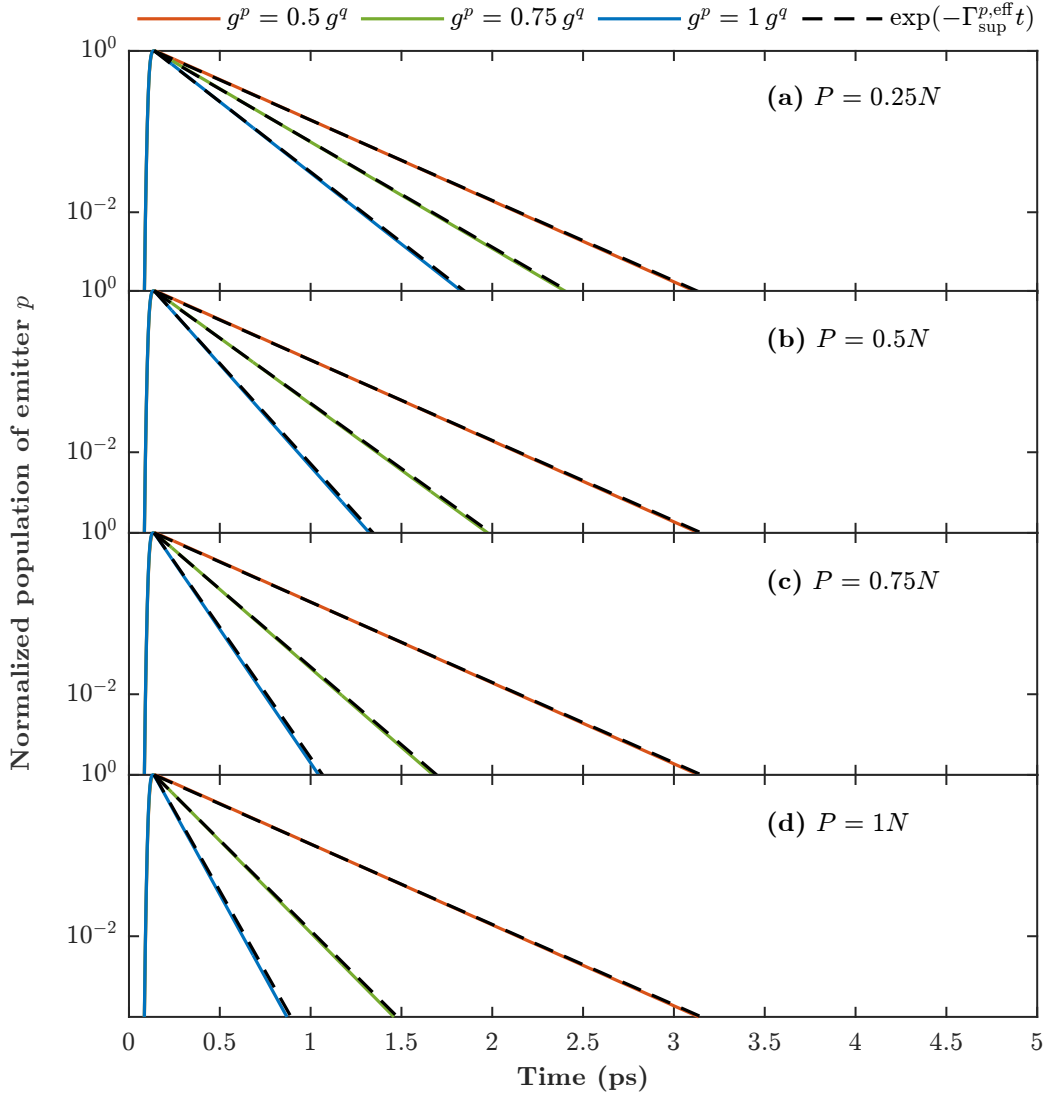


Fig. 7.1: Effect of introducing an asymmetry on the time evolution of the normalized population of the emitter p for the case of no pure dephasing. The asymmetry is introduced by considering two groups of emitters characterized by different coupling strength with the plasmon, g^p and g^q . The panels show the results for the ratio g^p/g^q being 1 (red solid line), 1.5 (green solid line) and 2 (blue solid line), and for different number P of emitters of the type p : (a) $P = 0.25N$, (b) $P = 0.5N$, (c) $P = 0.75N$ and (d) $P = 1N$, where $N = 20$ is the total number of emitters. The exponential decay with the rate Γ_{sup}^p [crefsup-eff] corresponding to the effective Purcell factor is shown by the black dashed lines. The parameters used for the simulation are $g^q = 3 \times 10^{12} \text{ s}^{-1}$, $\gamma_s^p = \gamma_s^q = 1 \times 10^9 \text{ s}^{-1}$, $\omega_0 = 3.14 \times 10^{15} \text{ s}^{-1}$, $\kappa = 3.14 \times 10^{14} \text{ s}^{-1}$, and $\omega_s^p = \omega_s^q = \omega_0$.

in the superradiant state which decays with rate Γ_{sup} [Eq. (7.1)], then subradiant states become populated due to dephasing and thus decay rate of the emitter is significantly decreased. By comparing decays for different value of g^p and same P , or for same value of g^p and different P , we can observe that relative weight of subradiant states decreases with increasing g^p and with increasing P , that is, when we increase the effective plasmon-emitter coupling strength (or effective Purcell factor P_F^{eff}). Thus, increasing the ratio between the coherent interaction and the pure dephasing increases the importance of the superradiant mode with respect to the subradiant ones. These results are consistent with those in Figs. 5.2 and 5.3, where the effective coupling strength was increased by considering more emitters in a symmetric situation.

7.2 System of non-identical emitters

In this section, we study decay of the ensemble of emitters coupled to each other via a silver nanoparticle, which is covered by a dielectric shell with a relative permittivity $\varepsilon_d = 1.5$ and thickness $d = 20$ nm. Emitters are randomly distributed over the dielectric shell. All emitters have a dipole moment of same size which corresponds to spontaneous decay rate $\gamma_s = 1 \times 10^9 \text{ s}^{-1}$, and they are oriented (a) radially or (b) tangentially to the surface. Coupling strength of each emitter to each of three dipolar plasmon modes of nanoparticle is determined using Eq. (2.18), where effective volume is given by Eq. (2.11) and scattered electric field by Eq. (4.14).

The system is illuminated by a linearly polarized plane wave, which excites one plasmon mode and emitters. To model coupling of the plasmon to the light we use $f = 10^8$ and we determine coupling strength of each emitter to the light Ω^i using Eq. (4.15) and values of f^β and $g^{i\beta}$.

Resonant frequency of a silver nanoparticle embedded in a medium with permittivity $\varepsilon_d = 1.5$ is given by Eq. (4.13). Using dielectric function of silver published by Johnson and Christy [26] we determine resonant frequency as $\omega_0 = 5.05 \times 10^{15} \text{ s}^{-1}$, which corresponds to light with the wavelength of 372 nm. For simplicity, we consider plasmon modes, emitters, and incident light to be in resonance. Moreover, using Eqs. (2.12) and (2.13) we determine the decay rate of plasmon $\kappa = 1.08 \times 10^{14} \text{ s}^{-1}$.

In Fig. 7.3 we show time evolution of the population of 20 emitters for different values of pure dephasing. The system of emitters with the radial polarization distributed as shown in Fig. 7.3(a) shows qualitatively same behaviour as symmetrical system discussed in Sections 5.1 and 5.2 – the system initially decays exponentially with a decay rate considerably larger than the spontaneous decay rate, and subsequently subradiant states become populated due to pure dephasing and the decay

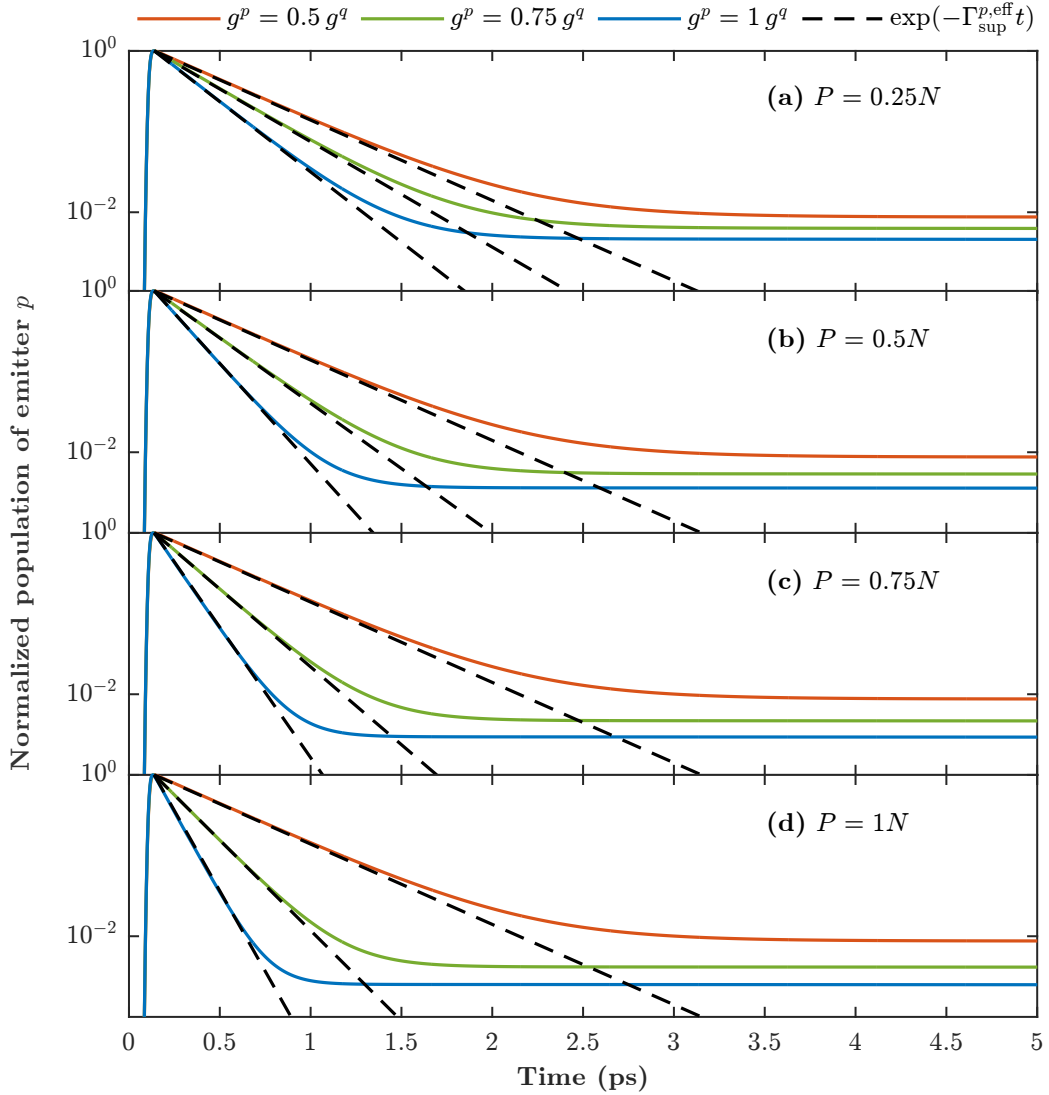


Fig. 7.2: Effect of introducing an asymmetry on the time evolution of the normalized population of the emitter p for the case of pure dephasing $\gamma_d^p = \gamma_d^q = 10\gamma_s$. The asymmetry is introduced by considering two groups of emitters characterized by different coupling strength with the plasmon, g^p and g^q . The panels show the results for the ratio g^p/g^q being 1 (red solid line), 1.5 (green solid line) and 2 (blue solid line), and for different number P of emitters of the type p : (a) $P = 0.25N$, (b) $P = 0.5N$, (c) $P = 0.75N$ and (d) $P = 1N$, where $N = 20$ is the total number of emitters. The exponential decay with the rate Γ_{sup}^p [crefsup-eff] corresponding to the effective Purcell factor is shown by the black dashed lines. The parameters used for the simulation are $g^q = 3 \times 10^{12} \text{ s}^{-1}$, $\gamma_s^p = \gamma_s^q = 1 \times 10^9 \text{ s}^{-1}$, $\omega_0 = 3.14 \times 10^{15} \text{ s}^{-1}$, $\kappa = 3.14 \times 10^{14} \text{ s}^{-1}$, and $\omega_s^p = \omega_s^q = \omega_0$.

rate of the system is decreased. Moreover, the decay rate of a subradiant state and its relative contribution to time evolution of the system increases with increasing dephasing. To find the decay rate of superradiant state we can utilize a standard equation for Purcell factor of the cavity [4] with an effective volume of plasmonic nanoparticle V_{eff} instead of a volume of cavity. The standard equation for Purcell factor corresponds to the situation in which emitter is at position of maximum enhancement of the electric field. Therefore, to get enhancement of the decay rate of the emitter at position \mathbf{r}_i we multiply standard Purcell factor by enhancement of the field at position of emitter $|\boldsymbol{\mu}_i \cdot \mathbf{E}^s(\mathbf{r}_i)|^2$ divided by maximum enhancement of the electric field $|\mathbf{E}_m^s|^2$. Purcell factor for system of M emitters is therefore

$$P_F^{\text{as}} = \frac{3Q}{4\pi^2 V_{\text{eff}}} \left(\frac{\lambda}{n}\right)^3 \sum_{i=1}^M \frac{|\boldsymbol{\mu}_i \cdot \mathbf{E}^s(\mathbf{r}_i)|^2}{|\mathbf{E}_m^s|^2} + 1, \quad (7.3)$$

where Q is quality factor of plasmonic resonance, λ is vacuum wavelength of emitted light and n is real part of refractive index of surrounding media. Exponential decay of the system with decay rate $P_F^{\text{as}}\gamma_s$, where Purcell factor P_F^{as} was computed for distribution of emitters shown in Fig. 7.3(a) is plotted by dashed line in the same figure. We observe good agreement of the time evolution computed using Purcell factor P_F^{as} with simulation for no pure dephasing (blue line).

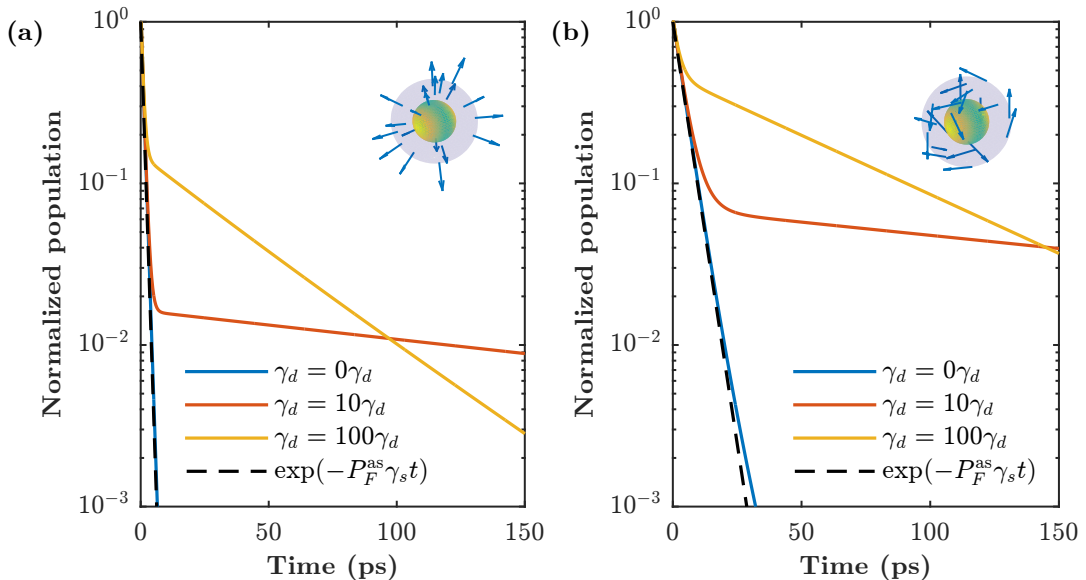


Fig. 7.3: Time evolution of the system of 20 emitters coupled to a plasmonic nanoparticle with the diameter $D = 20$ nm for different values of pure dephasing. The emitters are randomly distributed over a dielectric shell with the permittivity of 1.5 and the thickness $d = 10$ nm, dipole moments of the emitters are oriented (a) perpendicularly or (b) tangentially to the surface.

In Fig. 7.3(b) we consider a system with an identical spatial distribution of emitters as in Fig. 7.3(a), which have dipole moments oriented tangentially to the surface of the nanoparticle. From comparison of Fig. 7.3(a) and (b) it can be observed that enhancement of the spontaneous decay rate is considerably smaller if the emitters' dipole moments are oriented tangentially. Due to weaker enhancement subradiant states have larger contribution to the time evolution of the system with pure dephasing. Similar effect was already discussed in Section 5.1, where we observed increasing contribution of subradiant states with decreasing number of emitters in the system and thus decreasing enhancement of the superradiant decay rate. Furthermore, in the case of tangential distribution we observe biexponential decay even for system with no pure dephasing (blue line). This effect originates in the asymmetry of the system – for asymmetric system more than one superradiant state can exist – and can be in principle present also in case of perpendicular polarization. Nonetheless at least half of the decay of the system is sufficiently described by the superradiant state with the rate $P_F^{\text{as}}\gamma_s$. Nonetheless the decay of the system is sufficiently described by the superradiant decay rate until its average population reaches value of 0.5.

To conclude, the systems with asymmetry in coupling strength behave qualitatively very similarly to symmetric systems, except for the fact, that there can exist multiple superradiant states in asymmetric systems. Moreover, we can estimate the decay rate of the superradiant state of the system comprising non-identical emitters with known distribution using the modification of the standard expression for the Purcell factor Eq. (7.3).

8 EFFECT OF MUTUAL COUPLING BETWEEN EMITTERS

In Chapters 5–7 we studied systems of emitters which are coupled only via plasmon. Following the study of the system of non-identical emitters provided in Section 7.2 this chapter is focused on effect of direct mutual coupling between emitters.

We consider a system composed of 20 emitters with a spontaneous decay rate $\gamma_s = 1 \times 10^9 \text{ s}^{-1}$ and 3 dipolar plasmon modes of a silver nanoparticle with the decay rate $\kappa = 1.08 \times 10^{14} \text{ s}^{-1}$. Emitters are separated from the surface of the nanoparticle by a dielectric layer with a permittivity $\varepsilon_d = 1.5$ and a thickness d (which is varied between 10 nm and 40 nm in the following). A spatial distribution of the emitters over the surface of the dielectric shell is random. Plasmon-emitter coupling strength for each emitter is determined using Eqs. (2.18), (2.11), and (4.14). The system is excited by linearly polarized light, which couples only to one plasmon mode with the strength $f = 1 \times 10^8$, coupling between light and emitters is computed using Eq. (4.15).

First, we study an effect of direct coupling between emitters with radial orientation of dipole moments [see Fig. 8.1(a)] for different separation d between the emitters and the plasmonic nanoparticle (i.e. for different thickness of the dielectric shell) and for different values of pure dephasing. Let us first discuss the time evolution of the sum of the emitters' populations in the system without pure dephasing. When direct coupling is not considered (blue lines in Fig. 8.1) the emitters decay superradiantly. However, if the emitters couple also directly to each other (red lines in Fig. 8.1) the system first decay superradiantly and then the decay rate is significantly decreased. Due to direct coupling, energy is exchanged between the emitters and therefore the population of each emitter oscillates, as it is shown in Fig. 8.2. These oscillations are rather complex as the frequency of the energy exchange between each pair of emitters can be different. The resulting evolution of the sum of the emitters' populations, shown in Fig. 8.1, corresponds to superposition of N oscillations with different frequencies. Initially, individual emitters decay fast (see Fig. 8.2), namely the with the superradiant decay rate ($P_F^{\text{as}}\gamma_s$, see Section 7.2). As time evolves, emitters' decay rates become slower and oscillations dominate the time evolution of the emitters. Moreover, emitters become dephased because they oscillate at different frequencies, and the resulting decay rate of the system varies slowly and non-uniformly.

Fig. 8.1(b)–(e) shows time evolution of the system for different values of plasmon-emitters separation d . Systems of directly coupled emitters with no pure dephasing (red lines in different panels) become dephased at larger populations the larger is

distance d , thus the effect of direct coupling is more significant for the systems with larger distance between plasmonic nanoparticle and emitters. The explanation is following. The enhancement of the electric field at the position of the emitter responsible for the Purcell effect decays exponentially with its distance d from the nanoparticle, whereas coupling between the emitters decays as terms r^{-1} , r^{-2} , and r^{-3} with the distance r between them. The average distance between emitters is $\sqrt{4\pi/N}(d+R)$, where R is the radius of the nanoparticle. For a small distance d between the nanoparticle and the plasmon, average distance between emitters is much larger than plasmon-emitter distance, and therefore, plasmon-emitter interaction is stronger than mutual interaction between emitters.

Next, we study the effect of pure dephasing. Fig. 8.1 shows that by introducing pure dephasing (yellow and violet lines) the decay of the system becomes closer to exponential, because pure dephasing acts as damping of the oscillations of emitters. Note that similar effect was found for symmetric system in weak coupling regime (Chapter 6). With increasing pure dephasing damping of the oscillations increases and system approaches time evolution of the system without the mutual interaction between the emitters (dashed line for pure dephasing $\gamma_d = 10\gamma_s$ and dashed-dotted line for pure dephasing $\gamma_d = 100\gamma_s$). For pure dephasing $\gamma_d = 100\gamma_s$ the system with direct coupling between emitters evolves almost identically with the system of emitters coupled only via plasmon. Furthermore, we can observe that the larger is plasmon-emitter distance the less significant is direct coupling in the systems with pure dephasing – for plasmon-emitter distance $d = 40$ nm direct coupling is almost negligible even for pure dephasing $\gamma_d = 10\gamma_s$.

Let us now study the effect of direct coupling for tangential polarization of the system of emitters with identical spatial distribution as in Fig. 8.1. Orientation of emitters' dipole moments in the tangential plane is random. The system of tangentially oriented emitters behaves differently from the system with perpendicular orientation of emitters as can be observed in time evolutions of two emitters from the studied system shown in Fig. 8.3. In the case of tangential polarization we do not observe fast exponential decay, which was present in the case of radial polarization (see Fig. 8.2). The time evolution is governed by oscillations which have significantly larger frequency than the oscillations in the case of the perpendicular orientation, which results in faster dephasing of the emitters. As a result, by introducing direct coupling time evolution of the sum of populations of all emitters is changed dramatically – the system initially decays with a rate much smaller than the superradiant one – as it is shown by red lines in Fig. 8.4. The large difference between behaviour of the radial and the tangential polarization can be attributed to the fact, that deviation between the dipole moments of two emitters in the case of radial polarization is equal to their angular distance (with respect to the centre of

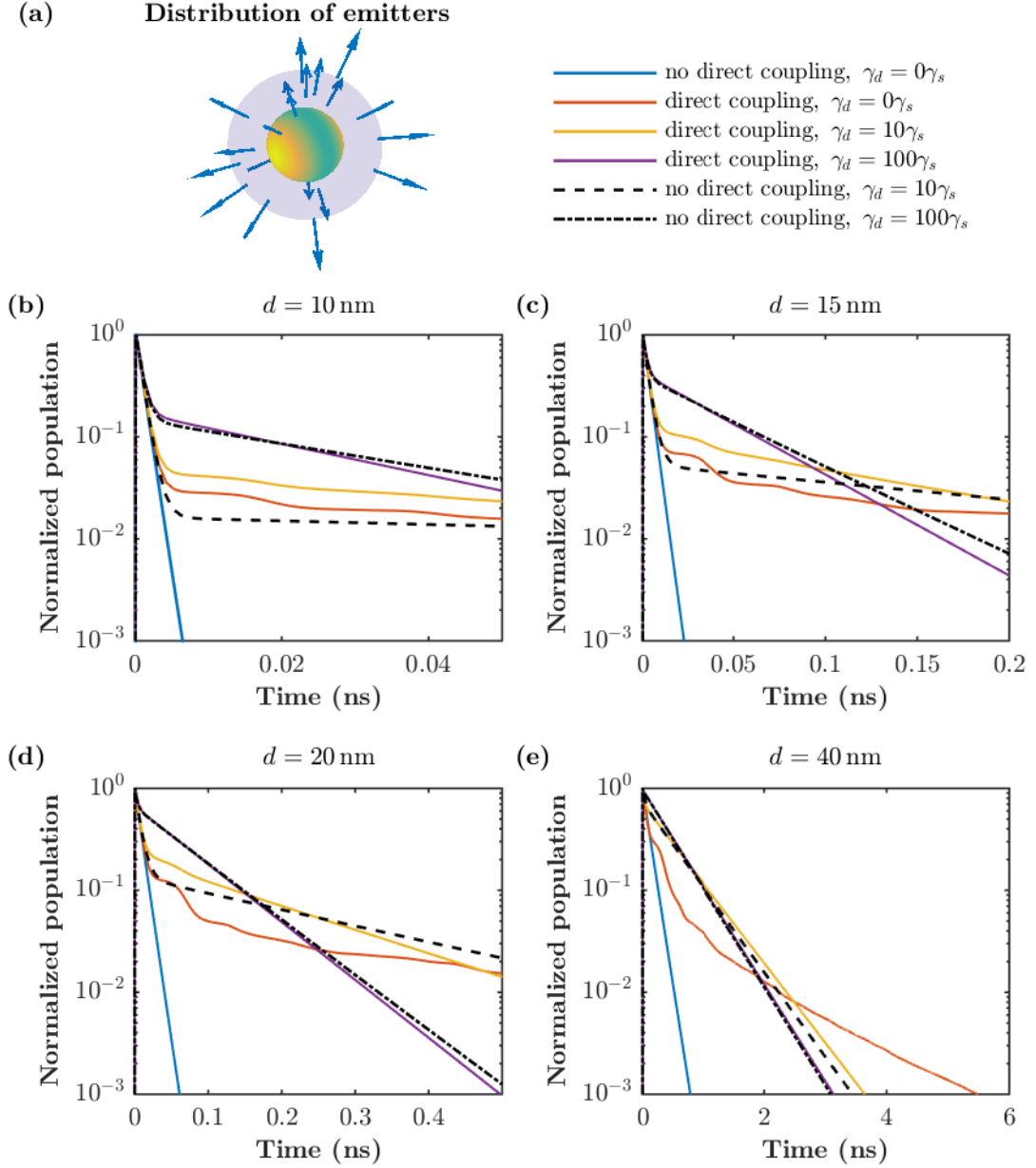


Fig. 8.1: (a) A system of 20 emitters coupled to a silver nanoparticle with the diameter $D = 20$ nm. Emitters with spontaneous decay rate $\gamma_s = 1 \times 10^9 \text{ s}^{-1}$ and with perpendicular orientation of dipole moments with respect to the nanoparticle surface are randomly distributed over a dielectric shell with the permittivity $\varepsilon_d = 1.5$. (b)–(e) Time evolution of the system of emitters separated from the nanoparticle by a distance (b) $d = 10$ nm, (c) $d = 15$ nm, (d) $d = 20$ nm, (e) $d = 40$ nm. Comparison of the system without direct coupling (blue lines) and with direct coupling (red lines) in case of no pure dephasing is provided. Moreover, time evolution of directly coupled emitters for dephasing $\gamma_d = 10\gamma_s$ (yellow lines) and $\gamma_d = 100\gamma_s$ (violet line) is compared with evolution of the same system without direct coupling (dashed line for $\gamma_d = 10\gamma_s$ and dashed-dotted line for $\gamma_d = 100\gamma_s$).

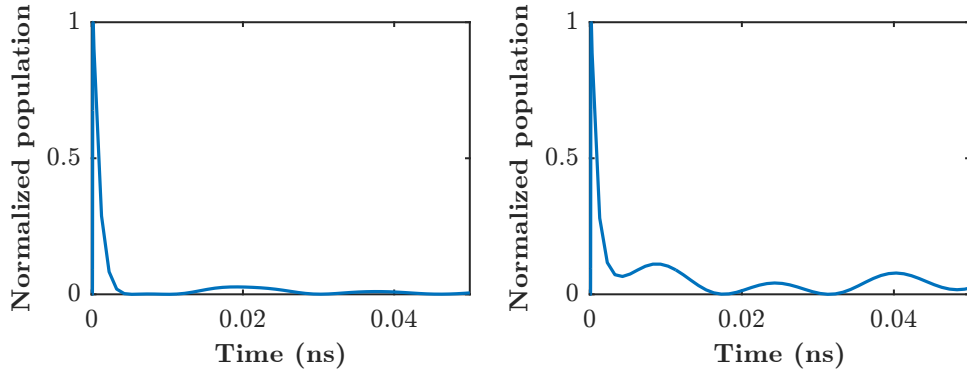


Fig. 8.2: Time evolution of two different emitters from an ensemble of 20 emitters coupled to each other directly and via a plasmon. The system is composed of a plasmonic nanoparticle with the diameter $D = 20$ nm covered by a dielectric shell with the permittivity of $\varepsilon_d = 1.5$ and the thickness $d = 10$ nm and the emitters randomly distributed over the shell with dipole moments oriented perpendicularly to the surface of the nanoparticle.

the nanoparticle), whereas in the case of tangential polarization the deviation can be very large even between two nearby emitters (as their orientation in the tangential plane is random).

Fig. 8.4 further shows time evolution of the system for different values of pure dephasing and plasmon-emitter distance. In the case of tangential orientation of emitters' dipole moments we observe similar behaviour as in the case of perpendicular orientation (Fig. 8.1). Fig. 8.4(b)-(e) shows that by increasing either pure dephasing or distance of emitters from nanoparticle direct coupling becomes less significant. This effect is even stronger than in case of perpendicular distribution as for pure dephasing $\gamma_d = 100\gamma_s$, direct coupling is negligible for distances 20 nm and 40 nm of emitters from nanoparticle. However, system never decays superradiantly in case of tangential orientation of directly coupled emitters.

To conclude, direct coupling causes mutual dephasing of the emitters which results in decrease of the decay rate of the system. The system of emitters with the transition dipole moments oriented perpendicularly to the surface of the plasmonic particle decays initially with the superradiant decay rate, and for very small plasmon-emitter distances direct coupling can be negligible. On the contrary, the system with the tangential orientation of the dipole moments never decays superradiantly and therefore direct coupling is significant even for small plasmon-emitter distances. For large plasmon-emitter distances systems of directly coupled emitters with either perpendicular or tangential orientation of the dipole moments behave as independent emitters.

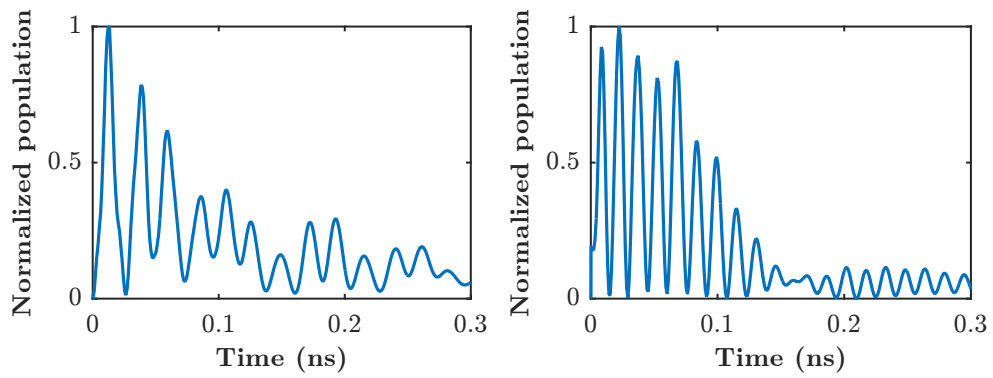


Fig. 8.3: Time evolution of two different emitters from an ensemble of 20 emitters coupled to each other directly and via a plasmon. The system is composed of a plasmonic nanoparticle with the diameter $D = 20$ nm covered by a dielectric shell with permittivity of $\epsilon_d = 1.5$ and thickness $d = 10$ nm and emitters randomly distributed over the shell with dipole moments oriented tangentially to the surface of the nanoparticle.

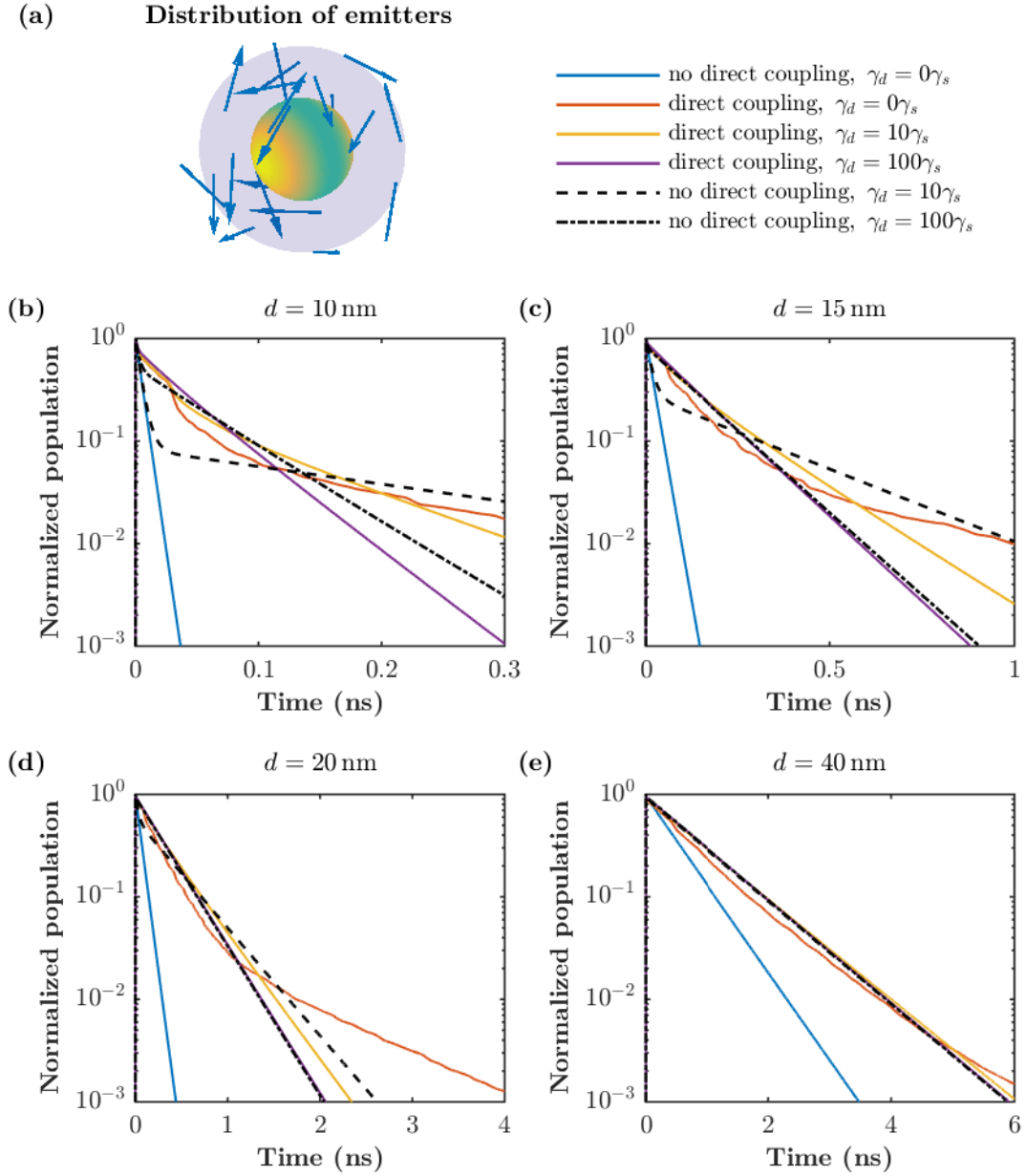


Fig. 8.4: (a) A system of 20 emitters coupled to a silver nanoparticle with the diameter $D = 20$ nm. Emitters with the spontaneous decay rate $\gamma_s = 1 \times 10^9 \text{ s}^{-1}$ and with tangential polarization are randomly distributed over a dielectric shell with the permittivity $\varepsilon_d = 1.5$. (b)–(e) Time evolution of the system of emitters separated from the nanoparticle by the distance (b) $d = 10$ nm, (c) $d = 15$ nm, (d) $d = 20$ nm, (e) $d = 40$ nm. Comparison of the system without direct coupling (blue lines) and with direct coupling (red lines) in case of no pure dephasing is provided. Moreover, time evolution of directly coupled emitters for dephasing $\gamma_d = 10\gamma_s$ (yellow lines) and $\gamma_d = 100\gamma_s$ (violet line) is compared with evolution of the same system without direct coupling (dashed line for $\gamma_d = 10\gamma_s$ and dashed-dotted line for $\gamma_d = 100\gamma_s$).

9 CONCLUSION

Light emission of a system comprising an ensemble of emitters coupled to a central plasmonic nanoparticle shows a phenomenon of plasmon-mediated superradiance – effect which combines the Purcell enhancement of spontaneous emission with a cooperative behaviour of coupled emitters. As a result, the decay rate of the system can be considerably enhanced, as was predicted by Pustovit and Shahbazyan [9]. We utilize a quantum model of emitters coupled to a plasmon to study time evolution of the system.

In this diploma thesis, we have first introduced a quantum description of an individual emitter coupled to a plasmon, and we have shown typical behaviour of such a system in weak and strong coupling regimes. For specific cases we have provided analytical solutions for time evolution of the system. We have also used a quantum model to describe classical (not mediated by plasmon) superradiance, which is an enhancement of the decay rate due to mutual coupling between emitters. The obtained results have been used to connect the quantum description with the classical predictions of the superradiant decay rate of emitters coupled via plasmon.

Following the description of simple systems, we have developed a complex model describing an arbitrary number of emitters coupled to several plasmon modes and excited by light illumination. First, we have studied a system of identical emitters at equivalent positions with respect to the nanoparticle. For the symmetric configuration in the weak coupling regime we have studied the effect of excitation and pure dephasing. We have shown that, although the type of excitation used does not affect the modes of the system, it determines which mode has a stronger contribution to the resulting time evolution. For example, if all dipoles are initially populated, a statistical mixture of a superradiant mode and subradiant modes is excited and a decay rate of the system does not increase with the number of emitters. On the other hand, when the plasmon is initially populated or excited by a short pulse, a superradiant mode dominates the response if pure dephasing is small enough. As the pure dephasing increases, but remains moderate, the contribution of the subradiant state becomes more apparent, and the decay rate of the system is significantly decreased. For very large values of pure dephasing the population of the emitter evolves as if only a single emitter was present.

In addition, we investigated how the symmetric system enters the strong coupling regime when the plasmon-emitter coupling strength and the number of emitters is sufficiently large. We have shown that an effective coupling strength, that takes into account the coupling of each emitter to the plasmon, allows to understand many of the obtained results. We also showed that increasing pure dephasing decreases the visibility and increases the damping of the Rabi oscillations.

Finally, we have focused on the effect of asymmetry in the plasmon-emitter coupling strength in the system of emitters randomly distributed over surface of a spherical nanoparticle covered by a dielectric shell. The decay rate of such a system depends on an actual distribution of emitters and orientation of their dipole moments. We have shown that for the known distribution, the superradiant decay rate can be determined using a modification of the standard equation for the Purcell factor of a cavity. Moreover, the effect of pure dephasing in an asymmetric configuration is qualitatively identical as in a symmetric system. We have also studied the effect of direct mutual coupling between emitters in the system. Direct coupling causes dephasing between the emitters, and therefore, the decay rate of the system become significantly decreased. Emitters located near the nanoparticle with dipole moments oriented perpendicularly to its surface decay mostly superradiantly and the effect of the direct coupling can be neglected. On the contrary, direct coupling dramatically changes the time evolution of the emitters with a tangential orientation of the dipole moments with respect to the nanoparticle. In such a system we do not observe superradiant decay.

Appendices

A ANALYTICAL SOLUTION FOR STRONG COUPLING

In Section 2.3.2 we introduced the strong coupling regime of the plasmon-emitter system as given by the system of Eqs. (2.21)–(2.24). For the case of no pure dephasing, this system can be solved analytically by finding the eigenvalues and eigenvectors of the system.

In this Appendix we present the full solution of the system in case of no dephasing ($\gamma_d = 0$). We note that analogical system of equations describing coupling of two non-identical emitters was presented in Ref. [27]. It is convenient to introduce the following notation

$$u = \frac{\gamma_s - \kappa}{4} \quad (\text{A.1})$$

$$B = \sqrt{\left(|g|^2 + u^2 + \frac{\Delta^2}{4}\right)^2 - 4|g|^2 u^2} \quad (\text{A.2})$$

$$D_{\pm} = \sqrt{2B \pm 2\left(u^2 - |g|^2 - \frac{\Delta^2}{4}\right)} \quad (\text{A.3})$$

$$(\text{A.4})$$

The general solution of the system is

$$\begin{pmatrix} \langle \hat{a}^\dagger \hat{a} \rangle \\ \langle \hat{\sigma}_+ \hat{a} \rangle \\ \langle \hat{\sigma}_- \hat{a}^\dagger \rangle \\ \langle \hat{\sigma}_+ \hat{\sigma}_- \rangle \end{pmatrix} = A_1 e^{\lambda_1} \mathbf{a}_1 + A_2 e^{\lambda_2} \mathbf{a}_2 + A_3 e^{\lambda_3} \mathbf{a}_3 + A_4 e^{\lambda_4} \mathbf{a}_4, \quad (\text{A.5})$$

where $\lambda_1, \lambda_2, \lambda_3, \lambda_4$ are eigenvalues

$$\begin{aligned} \lambda_1 &= -\frac{\kappa + \gamma_s}{2} - iD_-, & \lambda_2 &= -\frac{\kappa + \gamma_s}{2} + iD_-, \\ \lambda_3 &= -\frac{\kappa + \gamma_s}{2} - D_+, & \lambda_4 &= -\frac{\kappa + \gamma_s}{2} + D_+, \end{aligned} \quad (\text{A.6})$$

and $\mathbf{a}_1, \mathbf{a}_2, \mathbf{a}_3$ and \mathbf{a}_4 are eigenvectors

$$\mathbf{a}_1 = \begin{pmatrix} \frac{2u}{iD_-} + \frac{(2u - iD_-)\left(B - u^2 - \frac{\Delta^2}{4}\right)}{i|g|^2 D_-} \\ i \frac{(2u - iD_-)(D_- - \Delta)}{2gD_-} \\ -i \frac{(2u - iD_-)(D_- + \Delta)}{2g^* D_-} \\ 1 \end{pmatrix} \quad (\text{A.7})$$

$$\mathbf{a}_2 = \begin{pmatrix} -\frac{2u}{iD_-} - \frac{(2u + iD_-) \left(B - u^2 - \frac{\Delta^2}{4} \right)}{i|g|^2 D_-} \\ i \frac{(2u + iD_-) (D_- + \Delta)}{2gD_-} \\ -i \frac{(2u + iD_-) (D_- - \Delta)}{2g^* D_-} \\ 1 \end{pmatrix} \quad (\text{A.8})$$

$$\mathbf{a}_3 = \begin{pmatrix} \frac{2u}{D_+} - \frac{(2u - D_+) \left(B + u^2 + \frac{\Delta^2}{4} \right)}{|g|^2 D_+} \\ i \frac{(2u - D_+) (D_+ - i\Delta)}{2gD_+} \\ -i \frac{(2u - D_+) (D_+ + i\Delta)}{2g^* D_+} \\ 1 \end{pmatrix} \quad (\text{A.9})$$

$$\mathbf{a}_4 = \begin{pmatrix} -\frac{2u}{D_+} + \frac{(2u + D_+) \left(B + u^2 + \frac{\Delta^2}{4} \right)}{|g|^2 D_+} \\ i \frac{(2u + D_+) (D_+ + i\Delta)}{2gD_+} \\ -i \frac{(2u + D_+) (D_+ - i\Delta)}{2g^* D_+} \\ 1 \end{pmatrix} \quad (\text{A.10})$$

The particular solution for the case in which the emitter is initially excited and the plasmon is in the ground state gives the following time evolution of the population of emitter:

$$\begin{aligned} \langle \hat{\sigma}_+ \hat{\sigma}_- \rangle = \exp \left(-\frac{\kappa + \gamma_s t}{2} \right) \{ & \times \\ & \frac{1}{2} \left(1 - \frac{u^2 + \frac{\Delta^2}{4}}{B} \right) \cos D_- t + \frac{1}{2} \left(1 + \frac{u^2 + \frac{\Delta^2}{4}}{B} \right) \cosh D_+ t + \\ & \left. + \frac{D_- (D_+^2 - 4u^2)}{8Bu} \sin D_- t - \frac{D_+ (D_-^2 + 4u^2)}{8Bu} \sinh D_+ t \right\}. \quad (\text{A.11}) \end{aligned}$$

B SYSTEM OF EQUATIONS FOR ASYMMETRICAL CASE OF TWO GROUPS OF EMITTERS

In this Appendix we present the system of equations which describes time evolution of the system composed of one plasmon mode and two different groups of emitters where the emitters within each group are identical. In the system of Eqs. (4.6)–(4.10) in Chapter 4, we distinguish parameters and operators related to the two different groups by the indices p and q . The number of the emitters of type p and q is denoted P and Q , respectively. As the index p stands for arbitrary dipole from the p type, it is necessary to distinguish two types of operators composed of $\hat{\sigma}_+^p, \hat{\sigma}_-^p$:

1. Population of the arbitrary dipole of the type p , further denoted as $\hat{\sigma}_+^p \hat{\sigma}_-^p$.
2. Coherence of two distinct dipoles from the same group. In order to differentiate from the population, coherences will be further denoted as $\hat{\sigma}_+^p \hat{\sigma}_-^{p'}$.

Decay rates and transition frequencies of the p emitters are γ_s^p and ω_s^p , respectively. Parameters which refer to the coherent and incoherent exchange of energy between two distinct emitters of the same type are denoted as γ_c^{pp} and ω_c^{pp} . This notation is also used for dipoles of the type q in an analogous way.

By applying these considerations to the general set of Eqs. (4.6)–(4.10), we derived the following system of equations:

$$\begin{aligned} \frac{d\langle \hat{a}^\dagger \hat{a} \rangle}{dt} &= -\kappa \langle \hat{a}^\dagger \hat{a} \rangle - i(f e^{-i\omega t} \langle \hat{a}^\dagger \rangle - f^* e^{i\omega t} \langle \hat{a} \rangle) \\ &+ iP(g^p \langle \hat{\sigma}_+^p \hat{a} \rangle - g^{p*} \langle \hat{\sigma}_-^p \hat{a}^\dagger \rangle) \\ &+ iQ(g^q \langle \hat{\sigma}_+^q \hat{a} \rangle - g^{q*} \langle \hat{\sigma}_-^q \hat{a}^\dagger \rangle), \end{aligned} \quad (\text{B.1})$$

$$\frac{d\langle \hat{a} \rangle}{dt} = -\left(\frac{\kappa}{2} + i\omega_0\right) \langle \hat{a} \rangle - i f e^{-i\omega t} - iP g^{p*} \langle \hat{\sigma}_-^p \rangle - iQ g^{q*} \langle \hat{\sigma}_-^q \rangle, \quad (\text{B.2})$$

$$\begin{aligned} \frac{d\langle \hat{\sigma}_+^p \hat{a} \rangle}{dt} &= -\left\{ \frac{\kappa + \gamma_s^p}{2} + \gamma_d^p + i(\omega_0 - \omega_s^p) + (P-1) \left(\frac{\gamma_c^{pp}}{2} - i\omega_c^{pp} \right) \right\} \langle \hat{\sigma}_+^p \hat{a} \rangle \\ &- Q \left(\frac{\gamma_c^{qp}}{2} - i\omega_c^{qp} \right) \langle \hat{\sigma}_+^q \hat{a} \rangle - i(P-1) g^{p*} \langle \hat{\sigma}_+^p \hat{\sigma}_-^{p'} \rangle - iQ g^{q*} \langle \hat{\sigma}_+^p \hat{\sigma}_-^q \rangle \\ &+ i g^{p*} \langle \hat{a}^\dagger \hat{a} \rangle - i g^{p*} \langle \hat{\sigma}_+^p \hat{\sigma}_-^p \rangle - i(f e^{-i\omega t} \langle \hat{\sigma}_+^p \rangle - \Omega^{p*} e^{i\omega t} \langle \hat{a} \rangle), \end{aligned} \quad (\text{B.3})$$

$$\begin{aligned} \frac{d\langle \hat{\sigma}_+^q \hat{a} \rangle}{dt} &= -\left\{ \frac{\kappa + \gamma_s^q}{2} + \gamma_d^q + i(\omega_0 - \omega_s^q) + (Q-1) \left(\frac{\gamma_c^{qq}}{2} - i\omega_c^{qq} \right) \right\} \langle \hat{\sigma}_+^q \hat{a} \rangle \\ &- P \left(\frac{\gamma_c^{pq}}{2} - i\omega_c^{pq} \right) \langle \hat{\sigma}_+^p \hat{a} \rangle - iP g^{p*} \langle \hat{\sigma}_+^q \hat{\sigma}_-^p \rangle - i(Q-1) g^{q*} \langle \hat{\sigma}_+^q \hat{\sigma}_-^{q'} \rangle \\ &+ i g^{q*} \langle \hat{a}^\dagger \hat{a} \rangle - i g^{q*} \langle \hat{\sigma}_+^q \hat{\sigma}_-^q \rangle - i(f e^{-i\omega t} \langle \hat{\sigma}_+^q \rangle - \Omega^{q*} e^{i\omega t} \langle \hat{a} \rangle), \end{aligned} \quad (\text{B.4})$$

$$\begin{aligned}
\frac{d \langle \hat{\sigma}_+^p \hat{\sigma}_-^p \rangle}{dt} &= -i (g^p \langle \hat{\sigma}_+^p \hat{a} \rangle - g^{p*} \langle \hat{\sigma}_-^p \hat{a}^\dagger \rangle) - i (\Omega^p e^{-i\omega t} \langle \hat{\sigma}_+^p \rangle - \Omega^{p*} e^{i\omega t} \langle \hat{\sigma}_-^p \rangle) \\
&\quad - \gamma_s^p \langle \hat{\sigma}_+^p \hat{\sigma}_-^p \rangle - (P-1) \gamma_c^{pp} \langle \hat{\sigma}_+^p \hat{\sigma}_-^{p'} \rangle \\
&\quad - Q \left\{ \left(\frac{\gamma_c^{qp}}{2} - i\omega_c^{qp} \right) \langle \hat{\sigma}_+^q \hat{\sigma}_-^p \rangle + \left(\frac{\gamma_c^{pq}}{2} + i\omega_c^{pq} \right) \langle \hat{\sigma}_+^p \hat{\sigma}_-^q \rangle \right\},
\end{aligned} \tag{B.5}$$

$$\begin{aligned}
\frac{d \langle \hat{\sigma}_+^p \hat{\sigma}_-^{p'} \rangle}{dt} &= -i (g^p \langle \hat{\sigma}_+^p \hat{a} \rangle - g^{p*} \langle \hat{\sigma}_-^p \hat{a}^\dagger \rangle) - i (\Omega^p e^{-i\omega t} \langle \hat{\sigma}_+^p \rangle - \Omega^{p*} e^{i\omega t} \langle \hat{\sigma}_-^p \rangle) \\
&\quad - \{ (P-2) \gamma_c^{pp} + \gamma_s^p + 2\gamma_d^p \} \langle \hat{\sigma}_+^p \hat{\sigma}_-^{p'} \rangle - \gamma_c^{pp} \langle \hat{\sigma}_+^p \hat{\sigma}_-^p \rangle \\
&\quad - Q \left\{ \left(\frac{\gamma_c^{qp}}{2} - i\omega_c^{qp} \right) \langle \hat{\sigma}_+^q \hat{\sigma}_-^p \rangle + \left(\frac{\gamma_c^{pq}}{2} + i\omega_c^{pq} \right) \langle \hat{\sigma}_+^p \hat{\sigma}_-^q \rangle \right\},
\end{aligned} \tag{B.6}$$

$$\begin{aligned}
\frac{d \langle \hat{\sigma}_+^q \hat{\sigma}_-^q \rangle}{dt} &= -i (g^q \langle \hat{\sigma}_+^q \hat{a} \rangle - g^{q*} \langle \hat{\sigma}_-^q \hat{a}^\dagger \rangle) - i (\Omega^q e^{-i\omega t} \langle \hat{\sigma}_+^q \rangle - \Omega^{q*} e^{i\omega t} \langle \hat{\sigma}_-^q \rangle) \\
&\quad - \gamma_s^q \langle \hat{\sigma}_+^q \hat{\sigma}_-^q \rangle - (Q-1) \gamma_c^{qq} \langle \hat{\sigma}_+^q \hat{\sigma}_-^{q'} \rangle \\
&\quad - P \left\{ \left(\frac{\gamma_c^{pq}}{2} - i\omega_c^{pq} \right) \langle \hat{\sigma}_+^p \hat{\sigma}_-^q \rangle + \left(\frac{\gamma_c^{qp}}{2} + i\omega_c^{qp} \right) \langle \hat{\sigma}_+^q \hat{\sigma}_-^p \rangle \right\},
\end{aligned} \tag{B.7}$$

$$\begin{aligned}
\frac{d \langle \hat{\sigma}_+^q \hat{\sigma}_-^{q'} \rangle}{dt} &= -i (g^q \langle \hat{\sigma}_+^q \hat{a} \rangle - g^{q*} \langle \hat{\sigma}_-^q \hat{a}^\dagger \rangle) - i (\Omega^q e^{-i\omega t} \langle \hat{\sigma}_+^q \rangle - \Omega^{q*} e^{i\omega t} \langle \hat{\sigma}_-^q \rangle) \\
&\quad - \{ (Q-2) \gamma_c^{qq} + \gamma_s^q + 2\gamma_d^q \} \langle \hat{\sigma}_+^q \hat{\sigma}_-^{q'} \rangle - \gamma_c^{qq} \langle \hat{\sigma}_+^q \hat{\sigma}_-^q \rangle \\
&\quad - P \left\{ \left(\frac{\gamma_c^{pq}}{2} - i\omega_c^{pq} \right) \langle \hat{\sigma}_+^p \hat{\sigma}_-^q \rangle + \left(\frac{\gamma_c^{qp}}{2} + i\omega_c^{qp} \right) \langle \hat{\sigma}_+^q \hat{\sigma}_-^p \rangle \right\},
\end{aligned} \tag{B.8}$$

$$\begin{aligned}
\frac{d \langle \hat{\sigma}_+^p \hat{\sigma}_-^q \rangle}{dt} &= -i (g^q \langle \hat{\sigma}_+^p \hat{a} \rangle - g^{p*} \langle \hat{\sigma}_-^q \hat{a}^\dagger \rangle) - i (\Omega^q e^{-i\omega t} \langle \hat{\sigma}_+^p \rangle - \Omega^{p*} e^{i\omega t} \langle \hat{\sigma}_-^q \rangle) \\
&\quad - (P-1) \left\{ \left(\frac{\gamma_c^{pp}}{2} - i\omega_c^{pp} \right) \langle \hat{\sigma}_+^p \hat{\sigma}_-^q \rangle + \left(\frac{\gamma_c^{qp}}{2} + i\omega_c^{qp} \right) \langle \hat{\sigma}_+^p \hat{\sigma}_-^{p'} \rangle \right\} \\
&\quad - (Q-1) \left\{ \left(\frac{\gamma_c^{qp}}{2} - i\omega_c^{qp} \right) \langle \hat{\sigma}_+^q \hat{\sigma}_-^{q'} \rangle + \left(\frac{\gamma_c^{qq}}{2} + i\omega_c^{qq} \right) \langle \hat{\sigma}_+^p \hat{\sigma}_-^q \rangle \right\} \\
&\quad - \left(\frac{\gamma_c^{qp}}{2} + i\omega_c^{qp} \right) \langle \hat{\sigma}_+^p \hat{\sigma}_-^p \rangle - \left(\frac{\gamma_c^{qp}}{2} - i\omega_c^{qp} \right) \langle \hat{\sigma}_+^q \hat{\sigma}_-^q \rangle \\
&\quad - \left\{ \frac{\gamma_s^p + \gamma_s^q}{2} + \gamma_d^p + \gamma_d^q + i(\omega_s^q - \omega_s^p) \right\} \langle \hat{\sigma}_+^p \hat{\sigma}_-^q \rangle,
\end{aligned} \tag{B.9}$$

$$\begin{aligned}
\frac{d \langle \hat{\sigma}_+^p \rangle}{dt} &= - \left\{ (P-1) \left(\frac{\gamma_c^{pp}}{2} - i\omega_c^{pp} \right) + \frac{\gamma_s^p}{2} - i\omega_s^p + \gamma_d^p \right\} \langle \hat{\sigma}_+^p \rangle \\
&\quad - Q \left(\frac{\gamma_c^{qp}}{2} - i\omega_c^{qp} \right) \langle \hat{\sigma}_+^q \rangle + i g^{p*} \langle \hat{a}^\dagger \rangle + i \Omega^{p*} e^{i\omega t},
\end{aligned} \tag{B.10}$$

$$\begin{aligned}
\frac{d \langle \hat{\sigma}_+^q \rangle}{dt} &= - \left\{ (Q-1) \left(\frac{\gamma_c^{qq}}{2} - i\omega_c^{qq} \right) + \frac{\gamma_s^q}{2} - i\omega_s^q + \gamma_d^q \right\} \langle \hat{\sigma}_+^q \rangle \\
&\quad - P \left(\frac{\gamma_c^{qp}}{2} - i\omega_c^{qp} \right) \langle \hat{\sigma}_+^p \rangle + i g^{q*} \langle \hat{a}^\dagger \rangle + i \Omega^{q*} e^{i\omega t}.
\end{aligned} \tag{B.11}$$

BIBLIOGRAPHY

- [1] PELTON, M., AIZPURUA, J., AND BRYANT, G. Metal-nanoparticle plasmonics. *Laser & Photonics Reviews* 2 (2008), 136–159. doi: [10.1002/lpor.200810003](https://doi.org/10.1002/lpor.200810003).
- [2] MAIER, S. A. *Plasmonics: fundamentals and applications*, 1st ed. Springer, 2007.
- [3] TAMINIAU, T. H., STEFANI, F. D., SEGERINK, F. B., AND VAN HULST, N. F. Optical antennas direct single-molecule emission. *Nature Photonics* 2 (2008), 234–237. doi: [10.1038/nphoton.2008.32](https://doi.org/10.1038/nphoton.2008.32).
- [4] PURCELL, E. M. Spontaneous emission probabilities at radio frequencies. *Physical Review* 69 (1946), 681. doi: [10.1103/PhysRev.69.674.2](https://doi.org/10.1103/PhysRev.69.674.2).
- [5] TÖRMÄ, P., AND BARNES, W. L. Strong coupling between surface plasmon polaritons and emitters: a review. *Reports on Progress in Physics* 78 (2015), 3901. doi: [10.1088/0034-4885/78/1/013901](https://doi.org/10.1088/0034-4885/78/1/013901).
- [6] ESTEBAN, R., AIZPURUA, J., AND BRYANT, G. W. Strong coupling of single emitters interacting with phononic infrared antennae. *New Journal of Physics* 16 (2014), 013052. doi: [10.1088/1367-2630/16/1/013052](https://doi.org/10.1088/1367-2630/16/1/013052).
- [7] TRÜGLER, A., AND HOHENESTER, U. Strong coupling between a metallic nanoparticle and a single molecule. *Physical Review B* 77 (2008), 115403. doi: [10.1103/PhysRevB.77.115403](https://doi.org/10.1103/PhysRevB.77.115403).
- [8] BROOKE, P. G., MARZLIN, K.-P., CRESSER, J. D., AND SANDERS, B. C. Super- and subradiant emission of two-level systems in the near-dicke limit. *Physical Review A* 77 (2008), 033844. doi: [10.1103/PhysRevA.77.033844](https://doi.org/10.1103/PhysRevA.77.033844).
- [9] PUSTOVIT, V. N., AND SHAHBAZIAN, T. V. Plasmon-mediated superradiance near metal nanostructures. *Physical Review B* 82 (2010), 075429. doi: [10.1103/PhysRevB.82.075429](https://doi.org/10.1103/PhysRevB.82.075429).
- [10] PUSTOVIT, V. N., AND SHAHBAZIAN, T. V. Cooperative emission of light by an ensemble of dipoles near a metal nanoparticle: The plasmonic dicke effect. *Physical review letters* 102 (2009), 077401. doi: [10.1103/PhysRevLett.102.077401](https://doi.org/10.1103/PhysRevLett.102.077401).
- [11] MANDEL, L., AND WOLF, E. *Optical coherence and quantum optics*, 1st ed. Cambridge University Press, 1995.

- [12] NOVOTNY, L., AND HECHT, B. *Principles of nano-optics*, 1st ed. Cambridge University Press, 2006.
- [13] CARMICHAEL, H. J. *Statistical Methods in Quantum Optics 1: Master Equations and Fokker-Planck Equations*. Springer, 2003.
- [14] SCULLY, M. O., AND ZUBAIRY, M. S. *Quantum Optics*, 1st ed. Cambridge University Press, 1997.
- [15] SHORE, B. W., AND KNIGHT, P. L. The Jaynes-Cummings model. *Journal of Modern Optics* 40 (1993), 1195–1238. doi: [10.1080/09500349314551321](https://doi.org/10.1080/09500349314551321).
- [16] SAVAGE, C. M. Quantum optics with one atom in an optical cavity. *Journal of Modern Optics* 37 (1990), 1711–1725. doi: [10.1080/09500349014551941](https://doi.org/10.1080/09500349014551941).
- [17] AUFFÈVES, A., GERACE, D., GÉRARD, J.-M., SANTOS, M. F., ANDREANI, L., AND POIZAT, J.-P. Controlling the dynamics of a coupled atom-cavity system by pure dephasing. *Physical Review B* 81 (2010), 245419. doi: [10.1103/PhysRevB.81.245419](https://doi.org/10.1103/PhysRevB.81.245419).
- [18] BREUER, H.-P., AND PETRUCCIONE, F. *The theory of open quantum systems*, 1st ed. Oxford University Press, 2002.
- [19] CLEMENS, J. P., HORVATH, L., SANDERS, B. C., AND CARMICHAEL, H. J. Collective spontaneous emission from a line of atoms. *Physical Review A* 68 (2003), 023809. doi: [10.1103/PhysRevA.68.023809](https://doi.org/10.1103/PhysRevA.68.023809).
- [20] AKRAM, U., FICEK, Z., AND SWAIN, S. Decoherence and coherent population transfer between two coupled systems. *Physical Review A* 62 (2000), 013413. doi: [10.1103/PhysRevA.62.013413](https://doi.org/10.1103/PhysRevA.62.013413).
- [21] DICKE, R. H. Coherence in spontaneous radiation processes. *Physical Review* 93 (1954), 99. doi: [10.1103/PhysRev.93.99](https://doi.org/10.1103/PhysRev.93.99).
- [22] R is freeware programme used as an alternative to Matlab. <https://cran.r-project.org/>.
- [23] JACKSON, J. D. *Classical Electrodynamics*, 3rd ed. John Wiley & Sons, Inc, 1998.
- [24] WANG, F., AND SHEN, Y. R. General properties of local plasmons in metal nanostructures. *Physical Review Letters* 97 (2006), 206806. doi: [10.1103/PhysRevLett.97.206806](https://doi.org/10.1103/PhysRevLett.97.206806).

- [25] ROGOBETE, L., KAMINSKI, F., AGIO, M., AND SANDOGHDAR, V. Design of plasmonic nanoantennae for enhancing spontaneous emission. *Optics Letters* 32 (2007), 1623–1625. doi: [10.1364/OL.32.001623](https://doi.org/10.1364/OL.32.001623).
- [26] JOHNSON, P. B., AND CHRISTY, R. W. Optical constants of the noble metals. *Physical Review B* 6 (1972), 4370–4379. doi: [10.1103/PhysRevB.6.4370](https://doi.org/10.1103/PhysRevB.6.4370).
- [27] FICEK, Z., TANAS, R., AND KIELICH, S. Cooperative effects in the spontaneous emission from two non-identical atoms. *Optica Acta* 33 (1986), 1149–1160. doi: [10.1080/713822079](https://doi.org/10.1080/713822079).